Published in final edited form as:

Nature. 2019 March ; 567(7748): 414–419. doi:10.1038/s41586-019-1016-7.

Histone H3 trimethylation at lysine 36 guides m^{6}A RNA modification co-transcriptionally

Huilin Huang[1,2,13], **Hengyou Weng**[1,2,13], **Keren Zhou**[3,4,13], **Tong Wu**[5,13], **Boxuan Simen Zhao**[5,13], **Mingli Sun**[1,6], **Zhenhua Chen**[1], **Xiaolan Deng**[1,2,6], **Gang Xiao**[1], **Franziska Auer**[1], **Lars Klemm**[1], **Huizhe Wu**[1,2,6], **Zhixiang Zuo**[2,7], **Xi Qin**[1,2], **Yunzhu Dong**[8], **Yile Zhou**[8], **Hanjun Qin**[9], **Shu Tao**[9], **Juan Du**[9], **Jun Liu**[5], **Zhike Lu**[5], **Hang Yin**[5], **Ana Mesquita**[2], **Celvie L. Yuan**[10], **Yueh-Chiang Hu**[10], **Wenju Sun**[3,4], **Rui Su**[1,2], **Lei Dong**[1,2], **Chao Shen**[1,2], **Chenying Li**[1,2], **Ying Qing**[1,2], **Xi Jiang**[1,2,11], **Xiwei Wu**[9], **Miao Sun**[12], **Jun-Lin Guan**[2], **Lianghu Qu**[3,4], **Minjie Wei**[6], **Markus Müschen**[1], **Gang Huang**[8,*], **Chuan He**[5,*], **Jianhua Yang**[3,4,*], and **Jianjun Chen**[1,2,*]

[1]Department of Systems Biology, Beckman Research Institute of City of Hope, Monrovia, CA 91016, USA

[2]Department of Cancer Biology, University of Cincinnati College of Medicine, Cincinnati, OH 45219, USA

[3]Key Laboratory of Gene Engineering of the Ministry of Education, Sun Yat-sen University, Guangzhou, Guangdong 510275, China

[4]State Key Laboratory for Biocontrol, Sun Yat-sen University, Guangzhou, Guangdong 510275, China

[5]Department of Chemistry, Department of Biochemistry and Molecular Biology, Institute for Biophysical Dynamics, Howard Hughes Medical Institute, University of Chicago, Chicago, IL 60637, USA

[*]Correspondence should be addressed to J.C., J.Y., C.H., G.H.. (jianchen@coh.org; yangjh7@mail.sysu.edu.cn; chuanhe@uchicago.edu; Gang.Huang@cchmc.org).

Author Contributions:

H.H., H.Weng, and J.C. conceived and designed the entire project. H.H., H.Weng, G.H., C.H., J.Y. and J.C. designed and supervised the research. H.H. and H.Weng prepared all samples for HT-seq, T.W. and B.S.Z. performed H3K36me3 ChIP-seq and m^{6}A-seq with input from H.Y., T.W. performed PAR-CLIP-seq, miCLIP-seq and ribosome profiling, H.Weng performed METTL14 ChIP-seq, H.H. performed mRNA stability profiling. H.H. and H.Weng performed dot blot and gene specific ChIP and MeRIP assays. H.H. and H.Weng prepared samples for LC-MS/MS while B.S.Z. and T.W. performed mass spectrometry. H.H. performed CLIP assays, gel shift, peptide pull-down, immunofluorescence, in vitro differentiation of mESCs, and gene expression correlation analyses. H.Weng isolated nascent RNA. H.H. and H.Weng performed MST. H.H. and H.Weng performed co-IP with the input from Z.C. H.H. performed western blot with the help of H.Weng, Mingli S., Z.C., X.D., H.Wu and X.Q. H.H. performed qPCR with the help of H.Weng, Mingli S., H.Wu and X.Q. G.X. designed sgRNAs and prepared dCas9 cell samples with the help of L.K. and F.A., while H.H. and H.Weng detected m^{6}A and H3K36me3 levels in specific loci. H.Weng constructed plasmids with the input from H.H., Mingli S. and X.Q. H.H. and H.Weng prepared all SETD2 KD and OE cell lines, A.M. established SETD2-KO Hela cells, F.A. established METTL14-KO HepG2 cells. Y.D., Y.Z. and G.H. provided Setd2-KO mice and Setd2 inducible KO mESCs. T.W. purified METTL3 and METTL14 recombinant protein with the help from J.L. Z.Z. performed integrated analysis of ChIP-seq and m^{6}A-seq data using public data. K.Z. analyzed all the genome-wide and transcriptome-wide data with input from W.S. and supervision from J.Y. and H.H. H.Q., S.T., J.D., C.Y., Y.H., R.S., L.D., C.S., C.L., Y.Q., X.J., X.W., Miao S., J.G., L.Q., M.W., M.M., G.H., C.H., J.Y., and J.C. contributed reagents/analytic tools and/or grant support; H.H., H.Weng and J.C. wrote the manuscript and all authors commented on the manuscript.

COMPETING FINANCIAL INTERESTS:

C.H. is a scientific founder and a scientific advisor board member of Accent Therapeutics, Inc.; J.C. is a scientific founder and the chief scientific officer of Genovel Biotech Corp. Both hold equities with their corresponding company.

[6]Department of Pharmacology, School of Pharmacy, China Medical University, Shenyang 110122, China

[7]Sun Yat-sen University Cancer Center, State Key Laboratory of Oncology in South China, Collaborative Innovation Center for Cancer Medicine, Guangzhou, 510060, China

[8]Divisions of Pathology and Experimental Hematology and Cancer Biology, Cincinnati Children's Hospital Medical Center, OH 45229, USA

[9]Intergrative Genomics Core, Beckman Research Institute of City of Hope, Monrovia, CA 91016, USA

[10]Division of Developmental Biology, Cincinnati Children's Hospital Medical Center, Cincinnati, OH 45229, USA

[11]Department of Pharmacology, and Bone Marrow Transplantation Center of the First Affiliated Hospital, Zhejiang University School of Medicine; Hangzhou, Zhejiang 310058, China

[12]Department of Pediatrics, University of Cincinnati College of Medicine; Division of Human Genetics, Cincinnati Children's Hospital Medical Center, Cincinnati, OH 45229, USA

[13]These authors contributed equally: Huilin Huang, Hengyou Weng, Keren Zhou, Tong Wu, Boxuan Simen Zhao.

Abstract

DNA and histone modifications exhibit noticeable impacts on gene expression[1]. Being the most prevalent internal modification in mRNA, *N*^{6}-Methyladenosine (m^{6}A) mRNA modification emerges as an important post-transcriptional mechanism of gene regulation[2-4] and plays critical roles in various normal and pathological bioprocesses[5-12]. However, how m^{6}A is precisely and dynamically deposited in the transcriptome remains elusive. Here we report that H3K36me3 histone modification, a marker for transcription elongation, globally guides m^{6}A modification. We found that m^{6}A modifications enrich in the vicinity of H3K36me3 peaks, and are reduced globally when cellular H3K36me3 is depleted. Mechanistically, H3K36me3 is recognized and bound directly by METTL14, a critical component of the m^{6}A methyltransferase complex (MTC), which in turn facilitates the binding of the m^{6}A MTC to adjacent RNA polymerase II, and thereby delivering the m^{6}A MTC to actively transcribed nascent RNAs to deposit m^{6}A co-transcriptionally. In mouse embryonic stem cells, phenocopying Mettl14 silencing, H3K36me3 depletion also induces m^{6}A reduction transcriptome-wide and in pluripotency transcripts, resulting in increased cell stemness. Collectively, our studies reveal the critical roles of H3K36me3 and METTL14 in determining precise and dynamic m^{6}A deposition in mRNA, and uncover another layer of gene expression regulation involving crosstalk between histone modification and RNA methylation.

Transcriptome-wide m^{6}A mapping reveals the presence of m^{6}A modification in approximately 7,000 mRNAs in both human and mouse transcriptomes and uncovers the consensus motif RRACH (R= G or A; H= A, C or U) in which A is converted to m^{6}A[13-15]. Despite the recognition of RRACH motifs by the METTL3-METTL14 methyltransferase complex *in vitro*, only a portion of them are methylated *in vivo*, which are typically enriched

in the coding sequence (CDS) and 3' untranslated region (UTR)[13-16]. How individual transcripts and specific sites are selected for proper deposition of m^{6}A modification remains elusive. Here we identified histone H3 trimethylation at lysine-36 (H3K36me3) as a determinant of m^{6}A RNA modification.

By comparing the distribution of m^{6}A in human transcriptome to that of different histone modifications, we found that 69.2% of m^{6}A peaks overlapped with the H3K36me3 modification (Extended Data Fig. 1a). Distance analysis also showed an overrepresentation of H3K36me3 modifications, but not H3K27me3 (as a control), near m^{6}A peaks (Extended Data Fig. 1b). Considering that H3K36me3 is the only known histone modification enriched in CDS and especially near the 3' end[17,18], these results revealed a possible unappreciated connection between H3K36me3 and m^{6}A RNA modification. Moreover, SET domain containing 2 (SETD2), the histone methyltransferase that specifically catalyzes H3K36me2 to H3K36me3[19], showed a positive correlation in mRNA expression with the m^{6}A MTC genes (i.e., *METTL3*, *METTL14* and *WTAP*) in most normal and cancer tissues/cell lines (Extended Data Fig. 1c-f). Suppression of cellular H3K36me3, either through knockdown/knockout of SETD2 or overexpression of KDM4A, one of the H3K36me3 demethylases[20], resulted in a significant decrease of m^{6}A level in total RNAs and/or poly(A) RNAs, comparable to the effects of depletion of each individual m^{6}A MTC genes (Fig. 1a and Extended Data Fig. 2a-k). This impact appears to be conserved in mammalian as heterozygous knockout of SETD2 in mouse c-kit$^+$ bone marrow cells also led to hypo-methylation of both H3K36me3 and m^{6}A (Extended Data Fig. 2l-o). In contrast, knockdown of SUV39H1, the H3K9me3 methyltransferase, did not affect m^{6}A abundance (Extended Data Fig. 2p-r). Gain-of-function experiments in SETD2-deficient A498 cells showed that the co-transcriptional catalytic activity of SETD2 is required for the restoration of H3K36me3 and m^{6}A levels (Fig. 1b and Extended Data Fig. 2s-u). On the other hand, however, silencing of m^{6}A MTC genes did not affect cellular H3K36me3 level (Extended Data Fig. 2v). Collectively, these results indicate a causal role of H3K36me3 on m^{6}A abundance and suggest that loss of H3K36me3 impaired *de novo* m^{6}A methylation.

Furthermore, we performed m^{6}A-seq in parallel with H3K36me3 ChIP-seq upon SETD2 knockdown to evaluate the global effect of H3K36me3 on m^{6}A deposition. ChIP-seq confirmed global reduction of H3K36me3, especially around stop codon, in SETD2 knockdown cells (Extended Data Fig. 3a-e). Meanwhile, m^{6}A-seq revealed a global hypomethylation of m^{6}A in the transcriptome upon SETD2 depletion (Fig. 1c and Extended Data Fig. 3f-i). Similarly, these m^{6}A-hypo peaks were mostly found in protein-coding mRNAs and enriched near stop codons (Extended Data Fig. 3j-k). Moreover, the most common m^{6}A consensus sequence "GGAC" was enriched in these m^{6}A-hypo peaks with the highest ratio (Extended Data Fig. 3l). Consistent results were also obtained with m^{6}A individual-nucleotide-resolution cross-linking and immunoprecipitation (miCLIP)[15] and subsequent sequencing (Extended Data Fig. 3m-q).

Integrated analysis of ChIP-seq and m^{6}A-seq data revealed that the chromosome position of H3K36me3 and m^{6}A were well correlated (z-score=212.93, P=9.99e-4, Permutation test; Extended Data Fig. 4a) and overlapped (Fig. 1d). Notably, the distributions of H3K36me3 and m^{6}A are mostly exclusive with that of heterochromatin markers H3K9me3 or

H3K27me3 (Extended Data Fig. 4a-c). Additional analyses revealed that the m^{6}A peaks associated with H3K36me3 modifications (H3K36me3+) are enriched near stop codon, while those without such association (H3K36me3-) are enriched around start codon (Extended Data Fig. 4d), indicating that H3K36me3 plays a role in m^{6}A determination preferentially at 3' end of CDS. On the other hand, 63% of H3K36me3+ loci were negative for m^{6}A modifications (m^{6}A-) and were found to enrich in CDS and intronic regions rather than 3' end (Extended Data Fig. 4e), consistent with the known functions of H3K36me3 in mediating deacetylation, preventing run-away transcription and regulating splicing[21-23]. In loci where H3K36me3 and m^{6}A are both present, 2,717 out of the 5,872 (46.3%) hypomethylated (FC<0.5) H3K36me3 peaks upon *SETD2* knockdown also exhibit hypomethylation (FC<0.5) of m^{6}A, while only 427 (7.3%) hypomethylated H3K36me3 peaks exhibit m^{6}A hypermethylation (FC>2). Such co-regulation of H3K36me3 and m^{6}A by SETD2 knockdown was confirmed in individual representative genes, such as *MYC*, *ACTB*, *KPNA6*, and *EEF1A* (Fig. 1e-f and Extended Data Fig. 4f-i), similar to what was observed when KDM4A was overexpressed (Extended Data Fig. 4j-k).

We further utilized CRISPR/dCas9-fusion, in which nuclease-deactivated Cas9 (dCas9) is guided by single guide RNAs (sgRNAs) and thus brings the fused protein to specific genomic regions for epigenetic modification[24], to confirm the casual regulation of H3K36me3 on m^{6}A on specific locus (Extended Data Fig. 5a-b). As expected, co-expression of dCas9-KDM4A fusion protein with sgRNAs (sgMYC) targeting the coding region instability determinant (CRD) region of MYC, where high level of H3K36me3 was observed (Fig. 1e), could partially remove H3K36me3 and subsequently impair m^{6}A deposition on *MYC* mRNA (Fig. 1g). On the other hand, co-expression of dCas9-SETD2 fusion with sgRNAs (sgGNG4) targeting the gene body of GNG4, where no detectable H3K36me3 and m^{6}A modifications were found (Extended Data Fig. 5c), increased H3K36me3 abundance in GNG4 gene body and m^{6}A modification in the corresponding mRNA region (Fig. 1h). Moreover, we also constructed an artificial fusion gene (MYC-GNG4) in which the 5' UTR sequence of GNG4 was fused downstream of MYC CRD (Extended Data Fig. 5d). We hypothesize that by fusing to MYC CRD, the H3K36me3 modification in GNG4 5' UTR sequence will be increased due to the elongation of pol II and co-transcriptional deposition of H3K36me3[25]. This was indeed the case, and more important, such fusion resulted in an elevated level of m^{6}A modification that could be partially or completely abrogated when SETD2 was depleted (Extended Data Fig. 5e), further demonstrating that m^{6}A modifications could be guided by H3K36me3.

We then compared the transcriptome-wide effect of SETD2 knockdown on m^{6}A to that caused by knockdown of individual m^{6}A MTC components (Fig. 2a). A given m^{6}A site that displayed more than 1.5-fold reduction upon knockdown of a given m^{6}A MTC gene was defined as the given MTC gene-responsive site. Among the SETD2-dependent m^{6}A-hypo sites, 84% were responsive to (the depletion of) one or more individual MTC genes (Fig. 2a). SETD2 silencing led to a global m^{6}A hypomethylation on METTL3-, METTL14-, or WTAP-responsive sites and particularly on the sites responsive to all three MTC genes (Fig. 2b), and such reduction mainly occurred within CDS and 3'UTR (Fig. 2c), as represented by *MYC* mRNA (Extended Data Fig. 6a). Moreover, significant positive correlation (r=0.51–0.60, P<2.22e-308) in the fold changes of m^{6}A abundance was observed between SETD2

knockdown and m^{6}A MTC gene knockdown (Fig. 2d). RNA-seq revealed that knockdown of SETD2 or individual MTC genes tend to suppress gene expression (Extended Data Fig. 6b), and their effects on the alterations of gene expression showed significant positive correlation (r=0.52–0.58, P<2.22e-308, Extended Data Fig. 6c). Further mRNA stability profiling and polysome profiling showed that SETD2 knockdown phenocopied METTL14 knockdown in affecting mRNA decay and translation (Extended Data Fig. 6d-h).

Mechanistically, we found that depletion of H3K36me3 by SETD2 silencing impaired the interaction between m^{6}A MTC proteins and their target mRNAs (Extended Data Fig. 7a), without affecting expression of individual m^{6}A MTC genes or the interaction between METTL3 and METTL14 (Extended Data Fig. 7b-f). These results imply that H3K36me3 plays a role in recruiting MTC to deposit m^{6}A marks on RNAs. Indeed, the *in vivo* interaction between H3K36me3 and individual m^{6}A MTC proteins was detected in a manner independent of RNA or DNA (Fig. 3a and Extended Data Fig. 7g-h). The binding appeared to be H3K36me3 specific as compared to H3K36me1 or H3K36me2 (Extended Data Fig. 7i). The interaction between H3K36me3 and endogenous METTL3/METTL14 was also validated (Extended Data Fig. 7j-k). Furthermore, silencing of individual m^{6}A MTC components *in cellulo* showed that depletion of METTL14, but not METTL3 or WTAP, impaired the interaction of MTC with H3K36me3 (Extended Data Fig. 7k), suggesting that METTL14 is key to the binding of MTC with H3K36me3. Importantly, the effect of SETD2 knockdown on m^{6}A reduction was largely impaired in the absence of METTL14 (Extended Data Fig. 7l).

Two possible models underlying this interaction, indirect (through adaptors) or direct (Reading and Writing, R/W) binding (Extended Data Fig. 8a), were then proposed. The indirect model was excluded because no known H3K36me3 readers (adaptors) tested could affect binding of H3K36me3 with METTL14 (Extended Data Fig. 8b-d). Instead, our *in vitro* (cell-free) pulldown assay and gel shift assay revealed a strong direct interaction between H3K36me3 and recombinant METTL14 protein (Fig. 3b and Extended Data Fig. 8e-f). Microscale thermophoresis (MST)[26,27] was then performed to evaluate the binding affinity, which gave an estimated Kd value of 1.860±0.288 μM (Fig. 3c).

To determine which region in METTL14 contributes to its binding with H3K36me3, we conducted truncation analysis using immunoprecipitation (Extended Data Fig. 8g). Among the truncations, Δ186–456 is the shortest variant that could interact with H3K36me3 (Extended Data Fig. 8g-h), suggesting that 1–185 amino acids are critical for the binding. Two fragments of METTL14, 138–143 and 153–161 amino acids, were further found to be important for the binding (Extended Data Fig. 8i). Functionally, only full length (FL), but not truncated variants of METTL14 (Δ138–143 or Δ153–161), could restore the m^{6}A abundance in METTL14 inducible knockout cells (Extended Data Fig. 8j).

Because METTL14 interacts with H3K36me3, we speculate that it also binds chromatin. Indeed, ChIP-seq with HA-tagged METTL14 using an HA antibody identified 1,973 peaks in HepG2 cells, among which 1,278 (65%) peaks were located in gene body (Fig. 3d). We further revealed genome-wide significant correlation between chromatin binding of METTL14 and H3K36me3, but not H3K27me3 (Fig. 3e and Extended Data Fig. 8k). In

addition, PAR-CLIP-seq revealed 5,981 potential METTL14 binding sites on RNA (Extended Data Fig. 8l-n). Distance analysis showed that METTL14 binding sites on RNA overlapped well with H3K36me3 and m^{6}A modification (Fig. 3f-g), supporting our proposed function of METTL14 in linking H3K36me3 with m^{6}A deposition.

In line with previous reports that H3K36me3 was established by SETD2 when associated with Pol II during transcription elongation[25], we demonstrated the association of m^{6}A MTC proteins with Pol II (Fig. 3a and Extended Data Fig. 7h), and specifically, the elongating form of Pol II (pSer2) (Extended Data Fig. 8o), and found that METTL14 co-localizes with H3K36me3 and pSer2-Pol II in the nucleus (Extended Data Fig. 8p), supporting a co-transcriptional regulation of H3K36me3 on m^{6}A. In addition, newly transcribed RNAs associated with chromatin exhibited higher abundance of m^{6}A modification than nucleoplasmic or cytoplasmic RNAs (Extended Data Fig. 8q). To better understand this process, we treated cells with a Pol II inhibitor 5,6-Dichlorobenzimidazole 1-β-D-ribofuranoside (DRB) for a short time. We found DRB decreased m^{6}A abundance without affecting H3K36me3 (Extended Data Fig. 8r-t). Notably, the interaction of METTL14 with H3K36me3, chromatin, or METTL3, was not interrupted by DRB treatment (Extended Data Fig. 8u-v). Therefore, our results suggest a working model in which METTL14, a critical component of the m^{6}A MTC, directly reads H3K36me3 in a Pol II independent manner, which allows the m^{6}A MTC to methylate adjacent nascent RNAs during Pol II-mediated transcription elongation (Fig. 3h).

Dynamic regulation of m^{6}A modifications is crucial for embryonic stem cells (ESCs) self-renewal and differentiation[5-7]. To decipher whether the regulation of H3K36me3 on m^{6}A RNA modification influences cell differentiation, we utilized the mouse ESC (mESC) model with doxycycline (Dox)-induced SETD2 knockdown for induction of *in vitro* differentiation through leukemia inhibitory factor (LIF) deprivation (Extended Data Fig. 9a-b). Upon Dox treatment, mESCs expressed higher levels of pluripotency factors, including OCT4, SOX2 and NANOG (Fig. 4a), and showed stronger staining of cell surface SSEA1 and nuclear OCT4 (Extended Data Fig. 9c), suggesting a more primitive state. On the other hand, the increase of endoderm markers (i.e., GATA4, GATA6, DAB2, and SOX7) during differentiation was attenuated in the presence of Dox (Extended Data Fig. 9d). The effects of SETD2 knockdown on mESC differentiation were similar to those caused by METTL14 knockdown (Extended Data Fig. 9e-g).

As expected, global H3K36me3 and cellular m^{6}A levels were substantially reduced in mESCs upon SETD2 knockdown (Extended Data Fig. 9h-m). Noticeably, most of the genes with H3K36me3 hypomethylation showed significantly reduced m^{6}A levels (Fig. 4b; P<2.22e-16 by Pearson's Chi-squared test), as represented by *SOX2* (Fig. 4c-d). Functional analysis of gene expression revealed the enrichment of stem cell maintenance genes in downregulated genes during LIF withdrawal and in upregulated genes upon SETD2 silencing (Extended Data Fig. 9n). In representative pluripotency genes with significant decrease of H3K36me3 upon Setd2 knockdown, an increase of m^{6}A level was observed during differentiation, which was prevented by Dox-induced SETD2 knockdown (Fig. 4e and Extended Data Fig. 9o). Consistent with the reported role of m^{6}A in destabilizing mRNAs (especially in ESCs)[2], these pluripotency genes showed a dramatic decrease in

mRNA level during differentiation, which could be partially rescued by SETD2 knockdown (Extended Data Fig. 9p). These results provide evidences that loss of H3K36me3 reduces m^6A in mESCs and delays *in vitro* differentiation. Furthermore, knockdown of METTL14 in SETD2-silenced cells could moderately further delay cell differentiation (Extended Data Fig. 10a-c). On the other hand, overexpression of METTL14 promoted differentiation in control cells, and could partially rescue differentiation inhibition in SETD2 knockdown cells (Extended Data Fig. 10d-f). Collectively, our results reveal that SETD2 and H3K36me3 inhibit pluripotency and promote differentiation of mESCs at least in part through regulation of m^6A on several critical pluripotency genes.

In summary, our results uncover a mechanism underlying the dynamic, precision and co-transcriptional deposition of m^6A modification in mammalian transcriptomes, explaining its prevalent occurrence to CDS and 3'UTR. The identification of the histone mark H3K36me3 as a determinant of m^6A RNA modification via METTL14 reveals a previously unknown cross-talk between histone modification and RNA methylation and therefore adds another layer of complexity to gene expression control in normal and pathological biological processes.

Extended Data

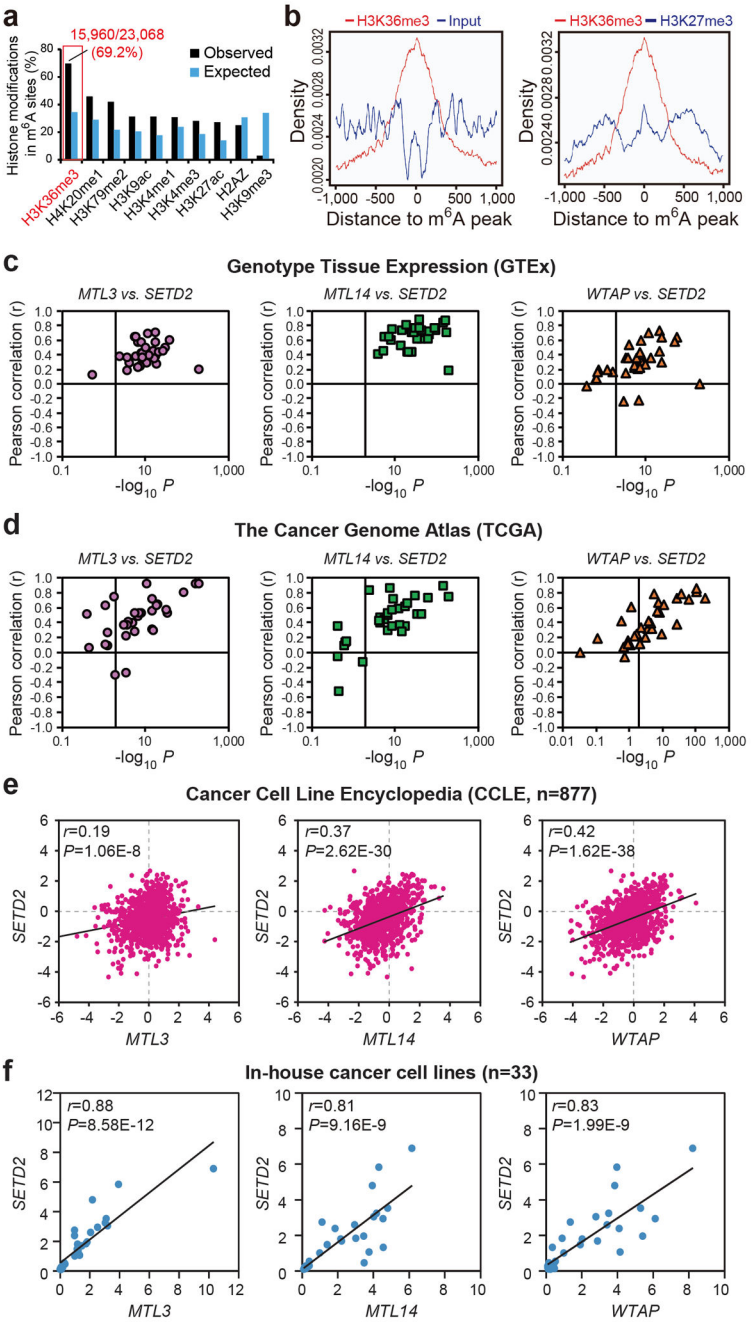

Extended Data Figure 1. Overlapping of H3K36me3 with m^{6}A and co-expression of their writer genes.

(a) Overlaps of m^{6}A sites with histone modification sites in human genome. Histogram showed the observed and expected percentages of m^{6}A sites that overlap with various histone modification sites; the ENCODE ChIP-seq data and m^{6}A-seq data (GSE37003) obtained from HepG2 cells were used for the analyses. (b) Distance of histone modifications to the nearest m^{6}A peaks. Input and H3K27me3 were shown as negative controls. (c-e)

Correlation of SETD2 with individual m^6A MTC genes (i.e., METTL3, METTL14, WTAP) in expression in normal tissues (c), cancer samples (d), and cell lines (e), based on the data from Genotype Tissue Expression (GTEx), The Cancer Genome Altlas (TCGA), and Cancer Cell Line Encyclopedia (CCLE) databases, respectively. Note that every dot represents one tissue type (c) or one cancer type (d). (f) Co-expression analysis of SETD2 and individual m^6A MTC genes in 33 cancer cell lines based on our qPCR data. The value of each gene represents relative expression as normalized to HEK293T cells. Correlation coefficient (*r*) and *P* value were calculated by Pearson's Correlation analysis in c, d, e and f.

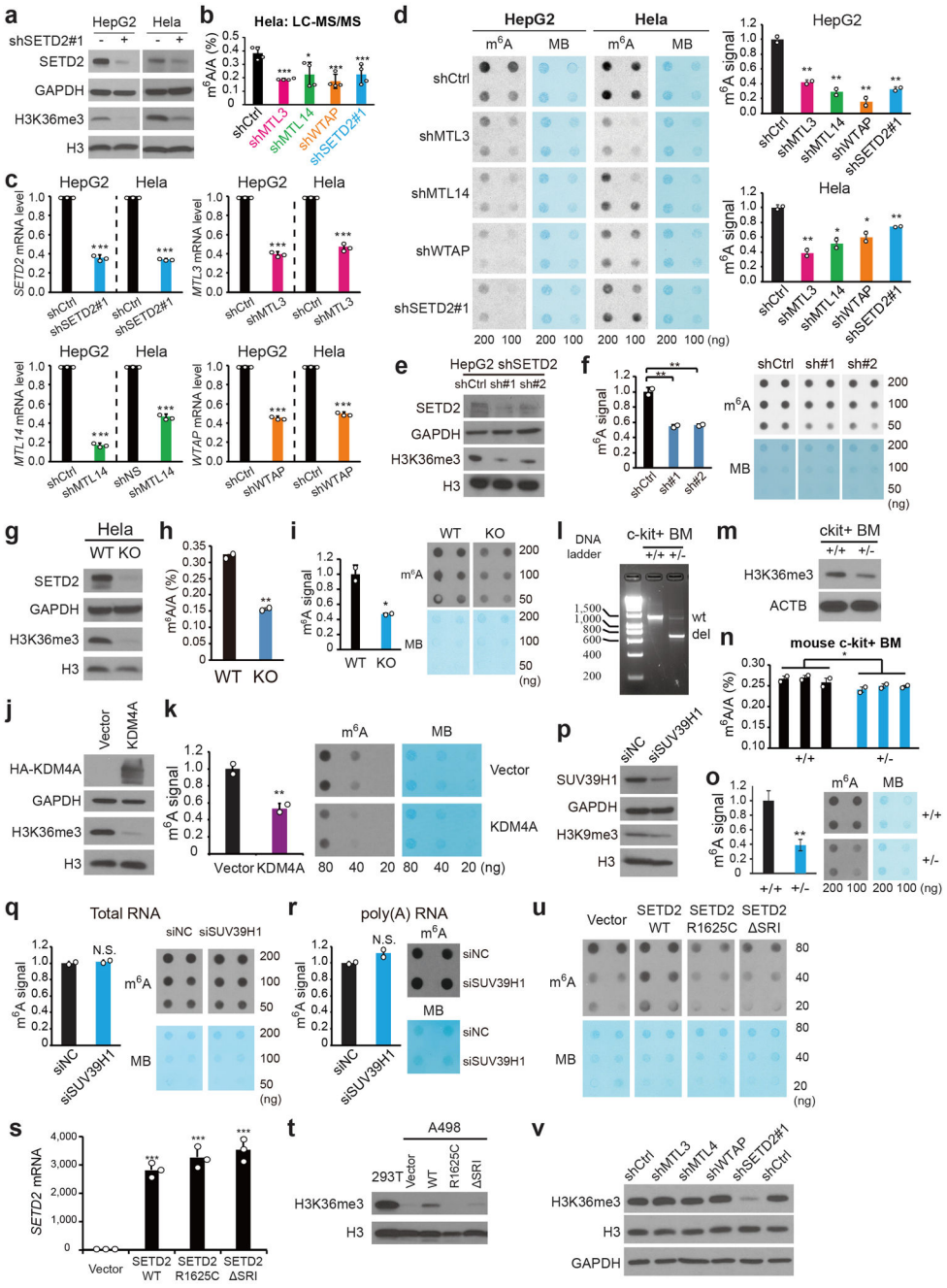

Extended Data Figure 2. Cellular m^{6}A level was regulated by the H3K36me3 methyltransferase SETD2 and the demethylase KDM4A.

(a) Western blot showing knockdown efficiency of SETD2 and decrease of H3K36me3 in HepG2 and Hela cells by shSETD2#1. GAPDH and H3 serve as loading controls. (b) LC-MS/MS quantification of m^{6}A abundance in poly(A) RNA from Hela cells with knockdown of SETD2 (shSETD2#1) or individual m^{6}A MTC genes compared to control cells. Values are mean±SD of two independent experiments. (c) Knockdown efficiency of shRNAs was verified by qPCR assays. Values are mean±SD of three independent experiments. (d) Dot blot (left) and quantification (right, values are mean±SD) of m^{6}A in total RNAs from control

cells or cells with knockdown of SETD2 or individual m^{6}A MTC genes. MB: methylene blue, serving as loading control. (e) Knockdown of SETD2 by two shRNAs were verified by western blot in HepG2 cells. (f) Dot blot (right) and quantification (left, values are mean ±SD) of m^{6}A in total RNAs from SETD2 knockdown HepG2 cells. (g) Western blot showing depletion of SETD2 and H3K36me3 in wild type (WT) or SETD2 knockout (KO) Hela cells. (h) LC-MS/MS quantification of m^{6}A in poly(A) RNA from WT or SETD2 KO Hela cells. Values are mean±SD of two independent experiments. (i) Dot blot (right) and quantification (left, values are mean±SD) of m^{6}A in total RNA from WT or SETD2 KO Hela cells. (j) Western blot confirmed the overexpression of HA-tagged KDM4A and decrease of H3K36me3 in HEK293T cells. (k) Quantification (left, values are mean±SD) and dot blot (right) showed hypomethylation of m^{6}A in poly(A) RNAs from HEK293T cells with KDM4A overexpression compared to control cells. (l) Genotyping of SETD2 heterozygous knockout (+/−) mice. c-kit+ bone marrow (BM) cells were used. (m) Western blot showing H3K36me3 level in c-kit+ BM cells from SETD2 heterozygous knockout (+/−) mice. (n and o) LC-MS/MS quantification (n) and dot blot analysis (o, values are mean±SD on left) of m^{6}A in poly(A) RNA from c-kit+ BM cells of wild type (+/+) and Setd2+/− mice. Values are mean±SD of two technical replications and 3 mice were used for each group in n. (p) Western blot showing expression of SUV39H1 and H3K9me3 in Hela cells transfected with siRNA against SUV39H1 (siSUV39H1) or negative control (siNC). (q and r) Dot blot and quantification (values are mean±SD on left) of m^{6}A in total RNA (q) or poly(A) RNA (r) from Hela cells transfected with siSUV39H1 or siNC. (s) A498 cells were transfected with GFP-fused wild type or mutated SETD2, and were selected for GFP positive cells after 48 hours by cell sorting. The elevation of SETD2 mRNA level in SETD2-overexpressed cells was confirmed by qPCR. Values are mean±SD of three independent experiments. (t) Western blot showing H3K36me3 level in A498 cells with (wild-type or mutant) or without SETD2 overexpression. HEK293T served as a positive control. (u) Dot blot detecting m^{6}A in poly(A) RNAs from A498 cells with (wild-type or mutant) or without SETD2 overexpression. (v) Western blot showing that silencing of individual m^{6}A MTC genes did not affect cellular H3K36me3 level. Two-tailed student's t-test was used in b, c, d, f, h, i, k, n, o, q, r and s; *, P<0.05; **, P<0.01; ***, P<0.001; N.S., non-significant. Images in a, d, g, and i were representative of three independent experiments, e, f, j, k, m, o, p, q, r, t, u and v were representative of two independent experiments. Source data of b, c, d, f, h, i, k, n, o, q, r and s are in Supplementary Table 4.

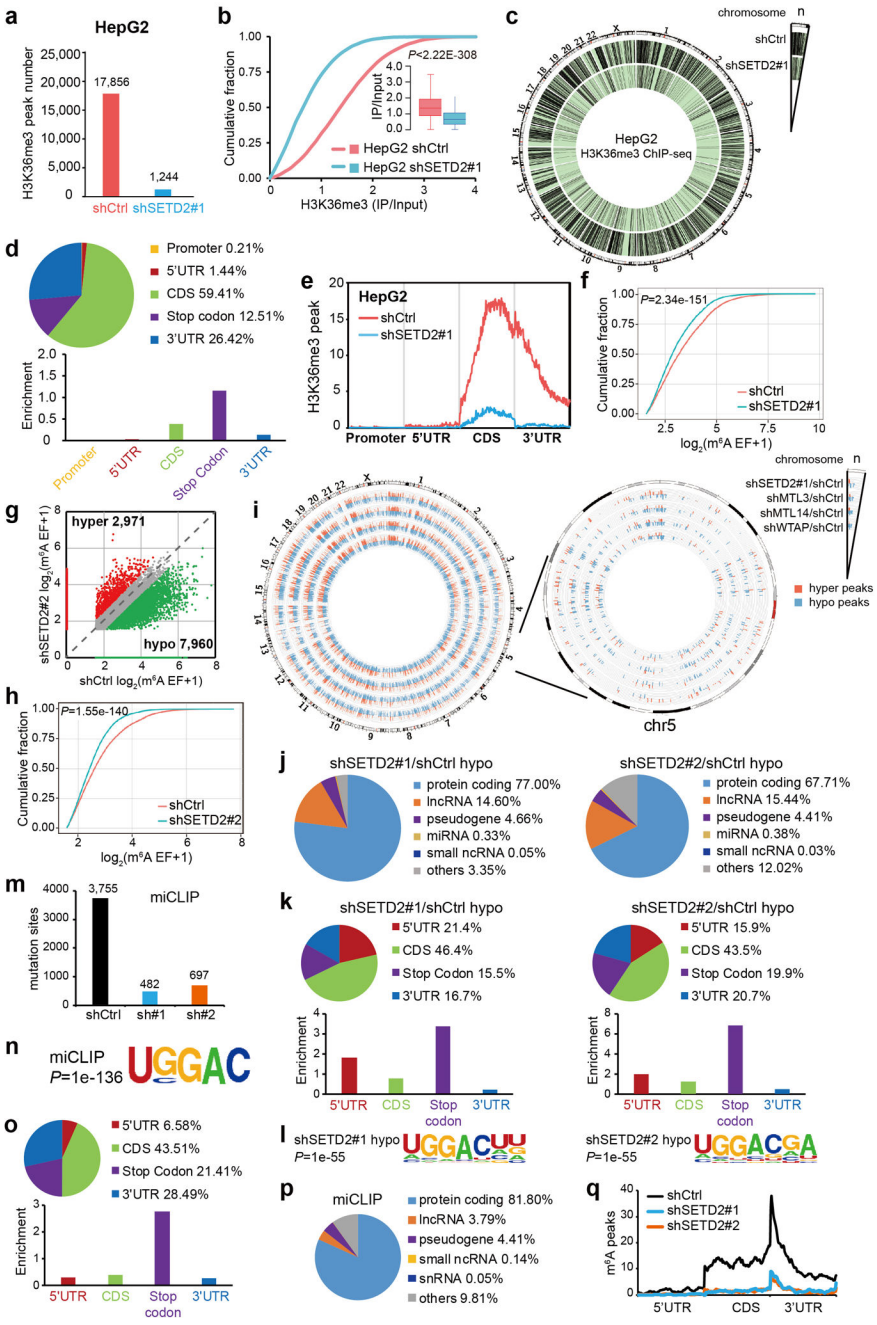

Extended Data Figure 3. Reprogramming of H3K36me3 and m^{6}A upon silencing of SETD2.

(a) Histogram showing H3K36me3 peak numbers in HepG2 cells with (shSETD2#1) or without (shCtrl) SETD2 knockdown. (b) Cumulative curves and box plot showing reduction of H3K36me3 in SETD2 knockdown HepG2 cells relative to control cells. *P* values were calculated using two-sided Wilcoxon and Mann-Whitney test. For the box plot, top of upper whisker is 95th percentile (shCtrl=3.436, shSETD2#1=2.073), top of the box is 75th percentile (shCtrl=1.898, shSETD2#1=1.035), line through the box is median (shCtrl=1.358, shSETD2#1=0.645), bottom of the box is 25th percentile (shCtrl=0.868, shSETD2#1=0.339), and bottom of the lower whisker is 5th percentile (shCtrl=0.001,

shSETD2#1=0.001). (c) Circos plot showing genome-wide decrease of H3K36me3 in SETD2 knockdown HepG2 cells compared to control cells. (d) The proportion (pie chart on top) and enrichment (histogram on bottom) of hypomethylated H3K36me3 peak distribution in the promoter, 5'UTR, CDS, stop codon, or 3'UTR region in SETD2 knockdown HepG2 cells. The enrichment was determined by the proportion of H3K36me3 peaks normalized by the length of the region. (e) Metagene profiles of H3K36me3 in SETD2 knockdown and control HepG2 cells. (f) Cumulative curves of m^6A abundance [i.e., $\log_2(m^6A\ EF+1)$] in control and SETD2 knockdown (shSETD2#1) HepG2 cells. Abundance of m^6A-IP was normalized to input when calculating the enrichment fold. *P* value was calculated using two-sided Wilcoxon and Mann-Whitney test. (g) Scatter plot of m^6A peaks in control (shCtrl) and SETD2 knockdown (shSETD2#2) HepG2 cells. The abundance of m^6A peaks was calculated as enrichment fold (EF, IP/input) from 3 independent m^6A-seq replications. Hypermethylated (hyper) peaks were in red, while hypomethylated (hypo) peaks were in green. (h) Cumulative curves of m^6A abundance [i.e., $\log_2$(enrichment fold+1)] in control and SETD2 knockdown (shSETD2#2) HepG2 cells. *P* value was calculated using two-sided Wilcoxon and Mann-Whitney test. (i) Circos plot showing the distribution of hypermethylated and hypomethylated m^6A peaks in human transcriptome (left) and chromosome 5 (right) upon knockdown of SETD2 or individual m^6A MTC genes. (j) Pie charts showing the percentages of hypomethylated m^6A peaks distribution in various RNA species by SETD2 knockdown in HepG2 cells. (k) The proportion (pie chart on top) and enrichment (histogram on bottom) of hypomethylated m^6A peak distribution in the 5'UTR, CDS, stop codon, or 3'UTR region in SETD2 knockdown HepG2 cells. The enrichment was determined by the proportion of m^6A peaks normalized by the length of the region. (l) HOMER motif analysis revealed conserved motifs enriched in hypomethylated peaks. *P* values were calculated by HOMER algorithm. (m) Numbers of m^6A sites in control (shCtrl) and SETD2 knockdown (sh#1 or sh#2) HepG2 cells identified by miCLIP. (n) HOMER motif analysis revealed conserved motifs of C to T mutations or truncations identified by miCLIP. *P* values were calculated by HOMER algorithm. (o) The proportion (pie chart on top) and enrichment (histogram on bottom) of miCLIP-identified m^6A distribution in gene body regions. (p) Percentages of various RNA species containing miCLIP-identified m^6A residues. (q) Metagene profiling of miCLIP-identified m^6A residues in control and SETD2 knockdown cells.

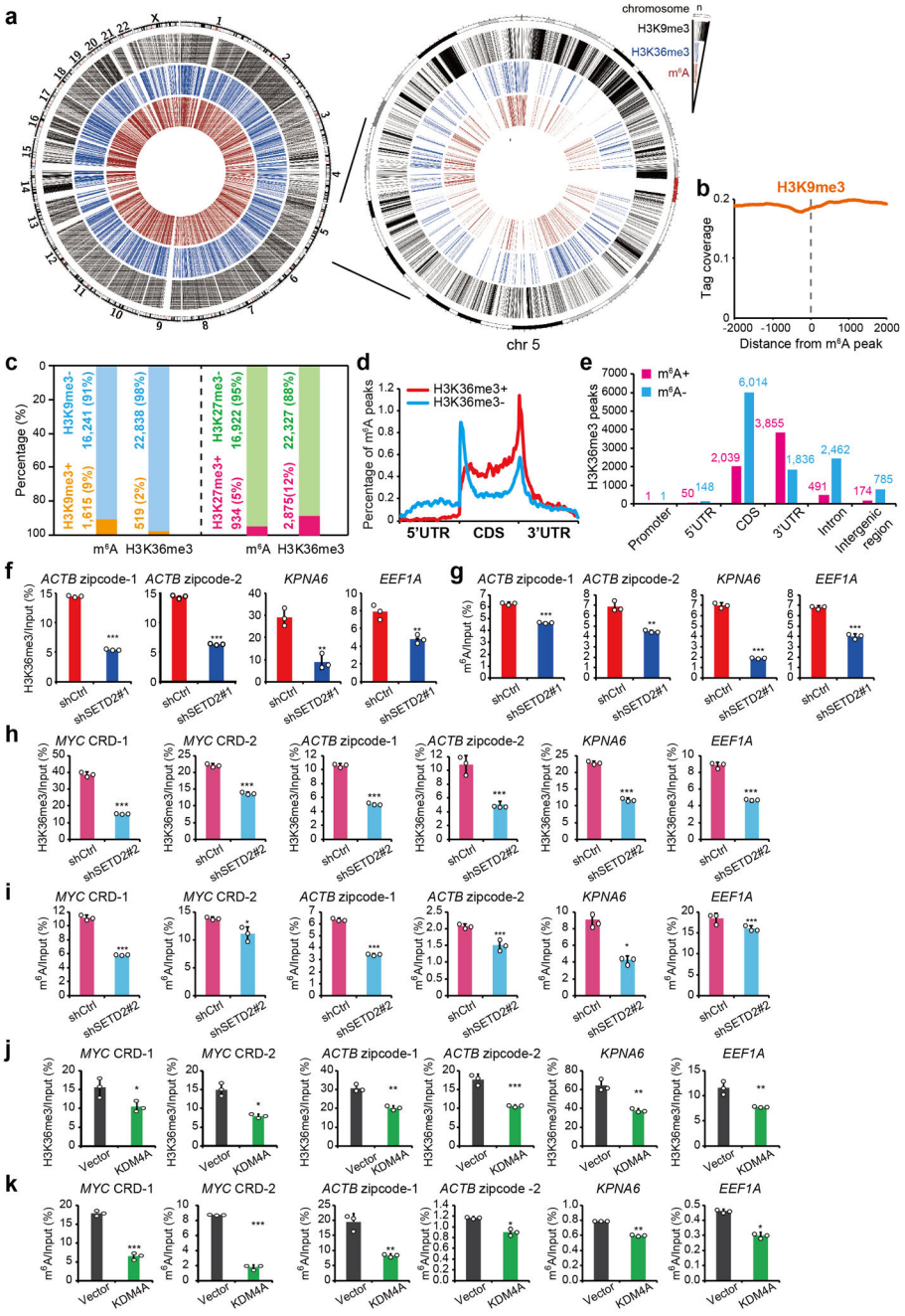

Extended Data Figure 4. Genome-/Transcriptome-wide and locus-specific co-regulation of H3K36me3 and m^{6}A.

(a) Circos plot showing global distribution of H3K36me3 and m^{6}A, as well as H3K9me3, in human genome (left) and chromosome 5 (right) of HepG2 cells. (b) Distribution of H3K9me3 relative to nearest m^{6}A sites in HepG2 cells. (c) Percentages and peak numbers of H3K36me3 and m^{6}A in H3K9me3 negative (H3K9me3-), H3K9me3 positive (H3K9me3+), H3K27me3 negative (H3K27me3-), or H3K27me3 positive (H3K27me3+) regions in HepG2 cells. (d) Distinct patterns of m^{6}A metagene at H3K36me3 positive (H3K36me3+) or negative (H3K36me3-) sites. (e) Distribution of H3K36me3 peaks with m^{6}A (m^{6}A+) or

without m^{6}A (m^{6}A-) modifications in gene body and intergenic regions. (f and g) Quantification of H3K36me3 (f) and m^{6}A (g) level in representative genes as determined by ChIP-qPCR and gene specific m^{6}A-qPCR assays in shSETD2#1 and control (shCtrl) HepG2 cells. (h and i) Quantification of H3K36me3 (h) and m^{6}A (i) level in representative genes as determined by ChIP-qPCR and gene specific m^{6}A-qPCR assays in shSETD2#2 and control (shCtrl) HepG2 cells. (j and k) Quantification of H3K36me3 (j) and m^{6}A (k) level in representative genes as determined by ChIP-qPCR and gene specific m^{6}A-qPCR assays in KDM4A-overexpressed and control HEK293T cells. Values are mean±SD of three independent experiments in f, g, h, i, j and k; two-tailed student's t-test; *, P<0.05; **, P<0.01; ***, P<0.001. Source data of f, g, h, i, j and k are in Supplementary Table 4.

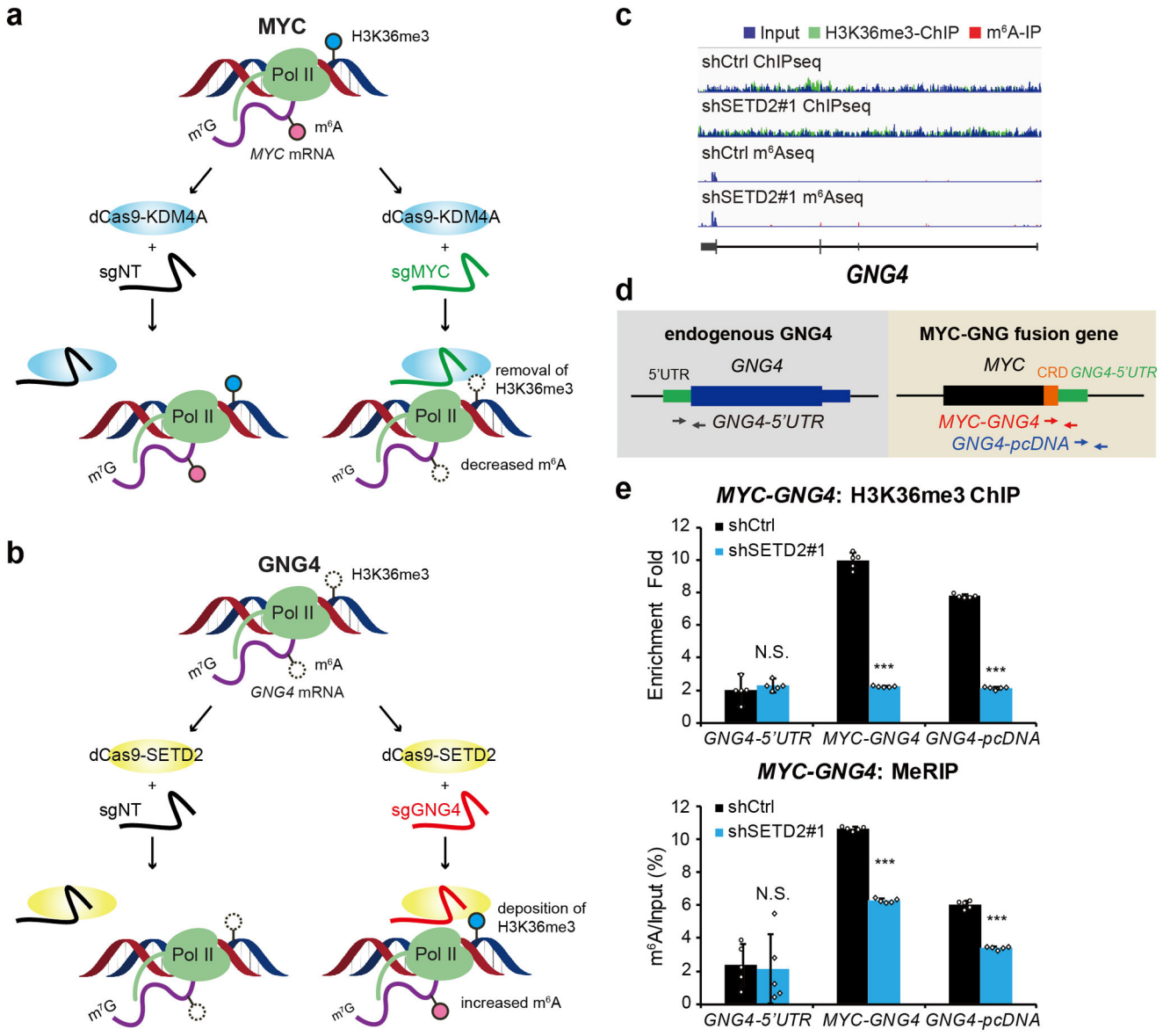

Extended Data Figure 5. Locus-specific regulation of m^{6}A by H3K36me3.

(a, b) Schematic showing the epigenetic editing of H3K36me3 by dCas9-KDM4A on MYC-CRD (a) or by dCas-SETD2 on GNG4 (b). (c) Distribution of H3K36me3 and m^6A peaks across *GNG4* mRNA transcript. (d) Schematic showing the endogenous GNG4 and artificial MYC-GNG4 fusion gene. The primers used to distinguish endogenous GNG4 (GNG4-5'UTR), MYC-GNG4 fusion sites (MYC-GNG4) or GNG4-vector fusion sites (GNG4-pcDNA) were indicated by black, orange, or blue arrows, respectively. (e) Quantification of H3K36me3 (top) and m^6A (bottom) in endogenous GNG4 or MYC-GNG4 fusion gene by ChIP-qPCR or gene specific m^6A assay in control or SETD2 knockdown cells. Values are mean±SD of five independent experiments. Two-tailed student's t-test was used; ***, $P<0.001$; N.S., non-significant. Source data of e are in Supplementary Table 4.

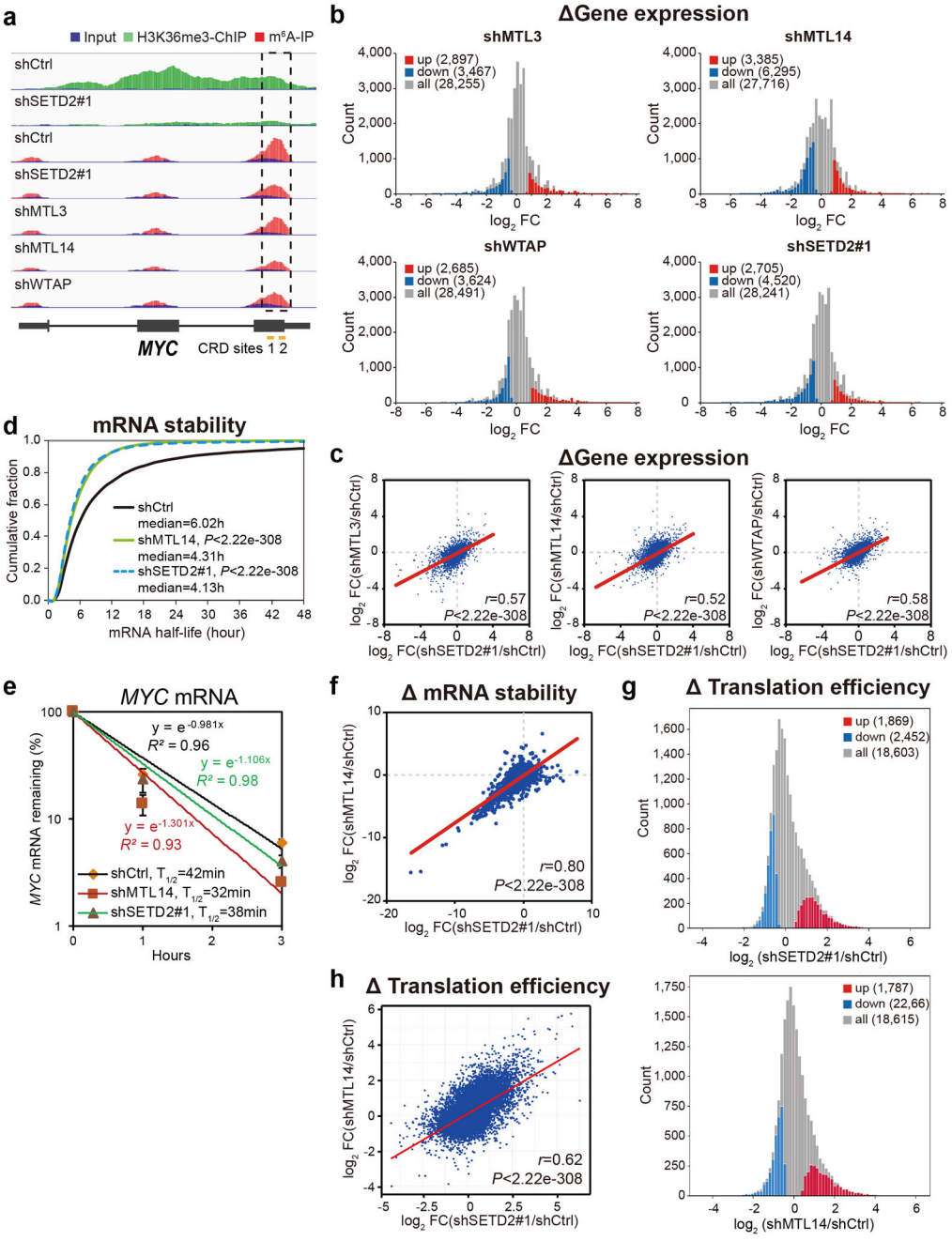

Extended Data Figure 6. Impact of SETD2 knockdown on gene expression, mRNA stability and translation.

(a) Distribution of H3K36me3 and m^{6}A peaks across *MYC* mRNA transcript. CRD: coding region instability determinant. (b) Histogram showing significant upregulated (up, $\log_2$FC>0.585, P<0.05) and downregulated (down, $\log_2$FC<−0.585, P<0.05) genes in SETD2 or individual MTC gene knockdown HepG2 cells. (c) Correlation of fold-change (FC) in gene expression between SETD2 knockdown and individual MTC gene knockdown cells. (d) Cumulative curves of mRNA half-life in SETD2 or METTL14 knockdown or control cells. P value was calculated using two-sided Wilcoxon and Mann-Whitney test. (e)

Decay curves and half-life ($T_{1/2}$) of *MYC* mRNA in SETD2 or METTL14 knockdown or control cells were derived from transcriptome-wide mRNA stability profiling. Values are mean±SD of two independent experiments. (f) Correlation of changes in mRNA half-life between SETD2 knockdown and METTL14 knockdown cells. (g) Histograms showing genes with significantly increase (up, $\log_2$FC>0.585, P<0.05) or decrease of translation efficiency (down, $\log_2$FC<−0.585, P<0.05) in SETD2 or METTL14 knockdown HepG2 cells. (h) Correlation of changes in translation efficiency between SETD2 knockdown and METTL14 knockdown cells. Correlation coefficient (r) and P values were calculated by Pearson's Correlation analysis in c, f and h. Source data of e are in Supplementary Table 4.

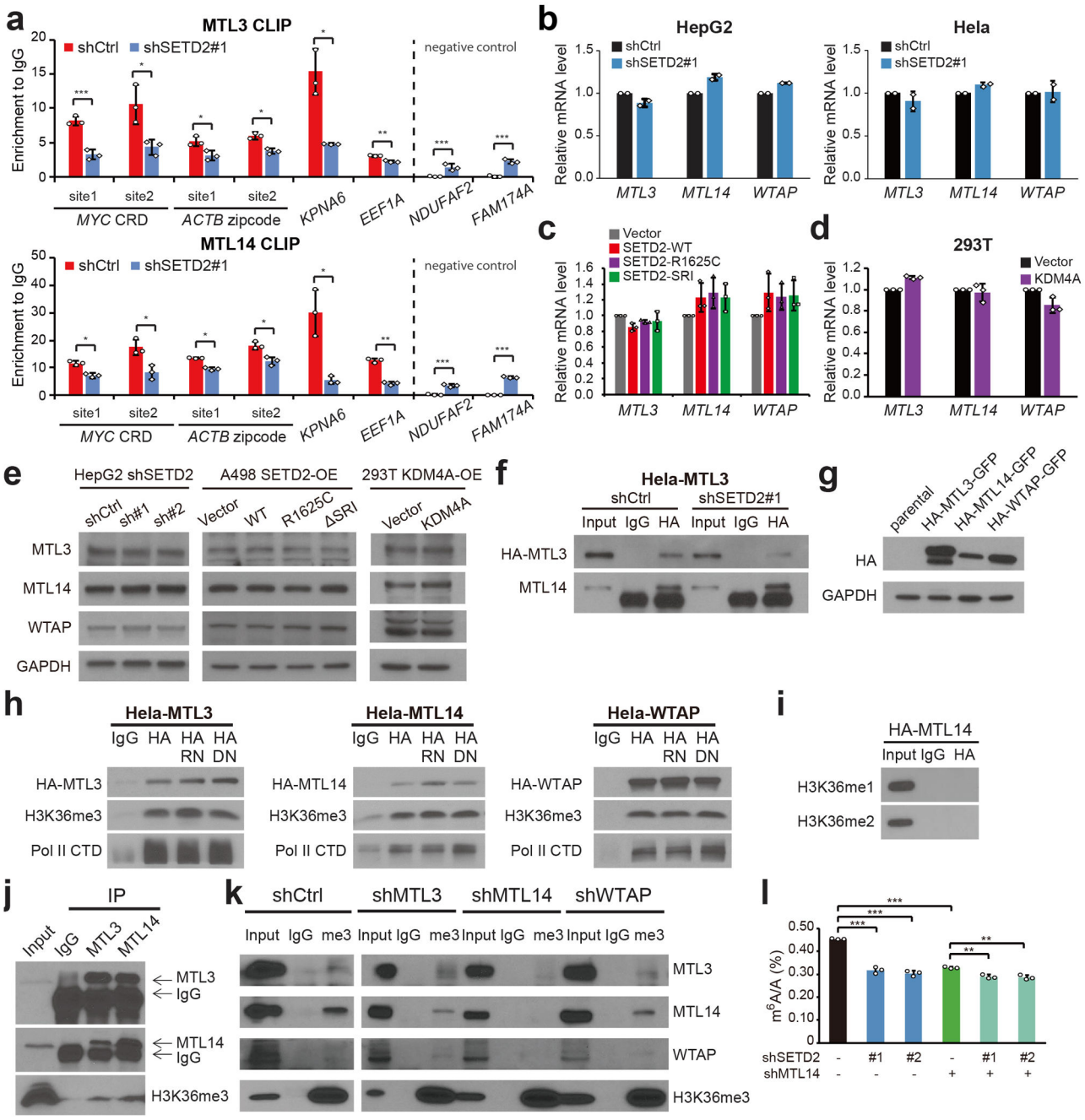

Extended Data Figure 7. Mechanism of H3K36me3-dependent m^{6}A modification.

(a) Binding of METTL3 (MTL3, upper panel) and METTL14 (MTL14, lower panel) to target mRNAs was determined by CLIP-qPCR assays. (b) qPCR data showing that knockdown of SETD2 in HepG2 and Hela cells did not downregulate the expression of m^{6}A MTC genes. (c) qPCR data showing that overexpression of SETD2 in A498 cells did not significantly change the expression of m^{6}A MTC genes. (d) qPCR showing that overexpression of KDM4A in HEK293T cells did not affect the expression of individual m^{6}A MTC genes i. GAPDH were used as reference gene when normalizing qPCR data in b, c and d. (e) Protein level of individual MTC in SETD2 silencing, SETD2 overexpression

(OE), or KDM4A overexpression cells was determined by western blot. (f) Interaction of METTL3 and METTL14 in SETD2 knockdown or control cells with forced expression of HA-METTL3. (g) Western blot showing forced expression of METTL3, METTL14, and WTAP in Hela cells. (h) Co-IP of HA-tagged individual m^6A MTC proteins in Hela cell lysates with or without pretreatment with DNase (DN, 100 U/ml) or RNase (RN, 2 ug/ml) for 1-hour at room temperature. (i) Co-IP of HA-tagged METTL14 showed no interaction between METTL14 and mono- or di-methylation of H3K36 (H3K36me1 and H3K36me2) in Hela cells. (j) Co-IP of endogenous METTL3 (M13) or METTL14 (M14) in Hela cells. The interaction between METTL3 or METTL14 with H3K36me3 was detected by western blot. (k) Co-IP of endogenous H3K36me3 in HepG2 cells without or with knockdown of individual m^6A MTC genes. (l) The m^6A/A ratio was quantified by LC-MS/MS in HepG2 cells with knockdown of SETD2 or/and METTL14. Values are mean±SD of two independent experiments in b and l and of three independent experiments in a, c and d; two-tailed student's t-test was used to test difference; *, $P<0.05$; **, $P<0.01$; ***, $P<0.001$. Images in e, f, g, h, i, j and k were representative of three independent experiments. Source data of a, b, c, d and l are in Supplementary Table 4.

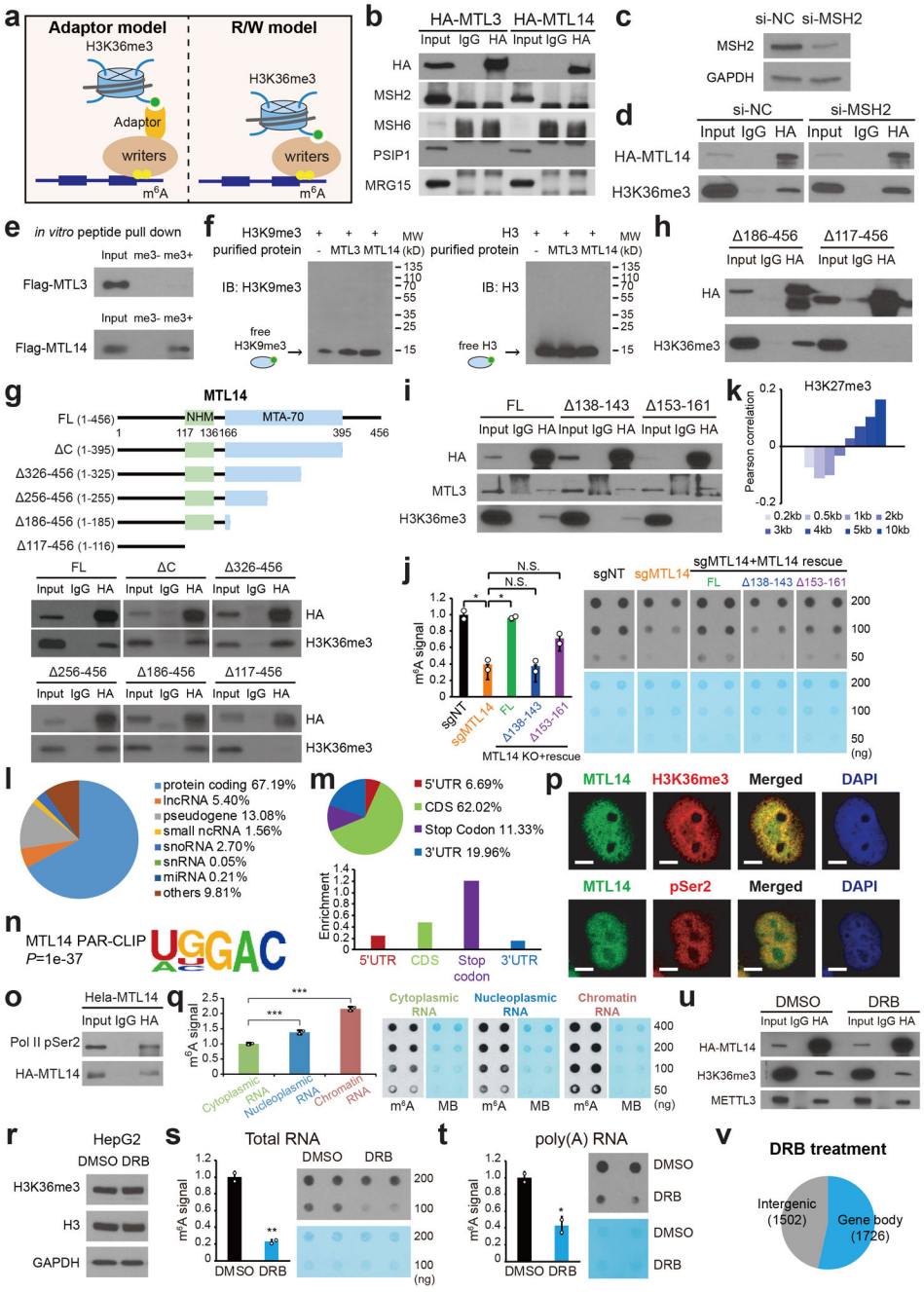

Extended Data Figure 8. METTL14 binds to H3K36me3 *in vitro* and *in vivo*.

(a) Schematic of the indirect or direct models of H3K36me3 recruiting MTC. “Adaptor” model (left) refers to indirect interaction of m^{6}A MTC with H3K36me3 through known H3K36me3 binding proteins (adaptors). “Reading and Writing” (R/W) model is shown on right, which proposes that m^{6}A writer complex functions as reader of H3K36me3 (green dot) and is recruited to chromatin to catalyze m^{6}A methylations (yellow dots) in newly synthesized RNAs. (b) Potential association of METTL3 or METTL14 with known H3K36me3 readers was examined by co-IP in Hela cells with forced expression of HA-tagged METTL3 or METTL14. (c) Western blot confirmed knockdown efficiency of MSH2

by siRNA. (d) Western blot showing that MSH2 siRNA did not affect the interaction between METTL14 and H3K36me3. (e) The direct binding of Flag-tagged recombinant human METTL3 or METTL14 proteins with histone 3 peptides with (me3+) or without (me3-) K36me3 modifications was examined by *in vitro* pull-down assays. (f) Gel shift of H3K9me3 or unmethylated histone H3 with recombinant human METTL3 or METTL14 in native SDS-PAGE gel. (g) Schematic of full-length (FL) METTL14 and its truncations was shown on top. Co-IP coupled with western blot showing the interaction of ectopically expressed FL or truncated METTL14 with H3K36me3 in Hela cells was shown on the bottom. (h) Co-IP coupled with western blot showed the interaction of ectopically expressed truncated (Δ186-456 or Δ117-456) METTL14 with H3K36me3 in HepG2 cells. (i) Co-IP coupled with western blot showed the interaction of ectopically expressed full length (FL) or truncated (Δ138-143 or Δ153-161) METTL14 with H3K36me3 in HepG2 cells. (j) m^6A Dot blot assays in METTL14 inducible knockout cells (sgMETTL14) transduced with different variants of METTL14. Images of m^6A and methylene blue blots were shown on right, while the quantification of m^6A was shown on left (values are mean±SD). (k) Pearson correlation coefficients of METTL14 ChIP-seq peaks with genomic H3K27me3 features in non-overlapping, non-repetitive windows of different sizes along the genome. (l) Percentages of various RNA species containing METTL14 binding sites detected by PAR-CLIP-seq. (m) The proportion (pie chart on top) and enrichment (histogram on bottom) of METTL14 CLIP binding sites distribution in gene body regions. (n) HOMER motif analysis of T to C mutations or truncations identified by METTL14 PAR-CLIP. *P* value was calculated by HOMER algorithm. (o) Co-IP showed that METTL14 bound to Ser2 phosphorylated polymerase II (Pol II pSer2) in Hela cells. (p) Co-localization of METTL14 with H3K36me3 (upper panels) or active transcription polymerase II (pSer2) (lower panels) in nuclei of HepG2 cells. Scale bar =10 μm. (q) Dot blot (right) and quantification (left, values are mean±SD) showing enrichment of m^6A in chromatin bound RNAs compared to that in RNAs from other cell fractions. (r) Western blot showing DRB treatment (100μM for 3 hours) did not affect H3K36me3 level in Hela cells. DMSO, was used as a vehicle control. (s and t) Dot blot and quantification (values are mean±SD on left) showing the m^6A abundance of total RNA (s) or poly(A) RNA (t) was reduced upon DRB treatment (at 100μM for 3 hours) in Hela cells. (u) Co-IP showing association of METTL14 with H3K36me3, METTL3 or Pol II CTD with or without DRB treatment. (v) Distribution of METTL14 binding sites on chromatin in DRB treated cells. Images in b, c, d, e, f, g, h, i, j, o, q, r, s, t and u were representative of three independent experiments. Two-tailed student's t-test was used to test difference in j, q, s and t; *, $P<0.05$; **, $P<0.01$; ***, $P<0.001$; N.S., non-significant. Source data of j, q, s and t are in Supplementary Table 4.

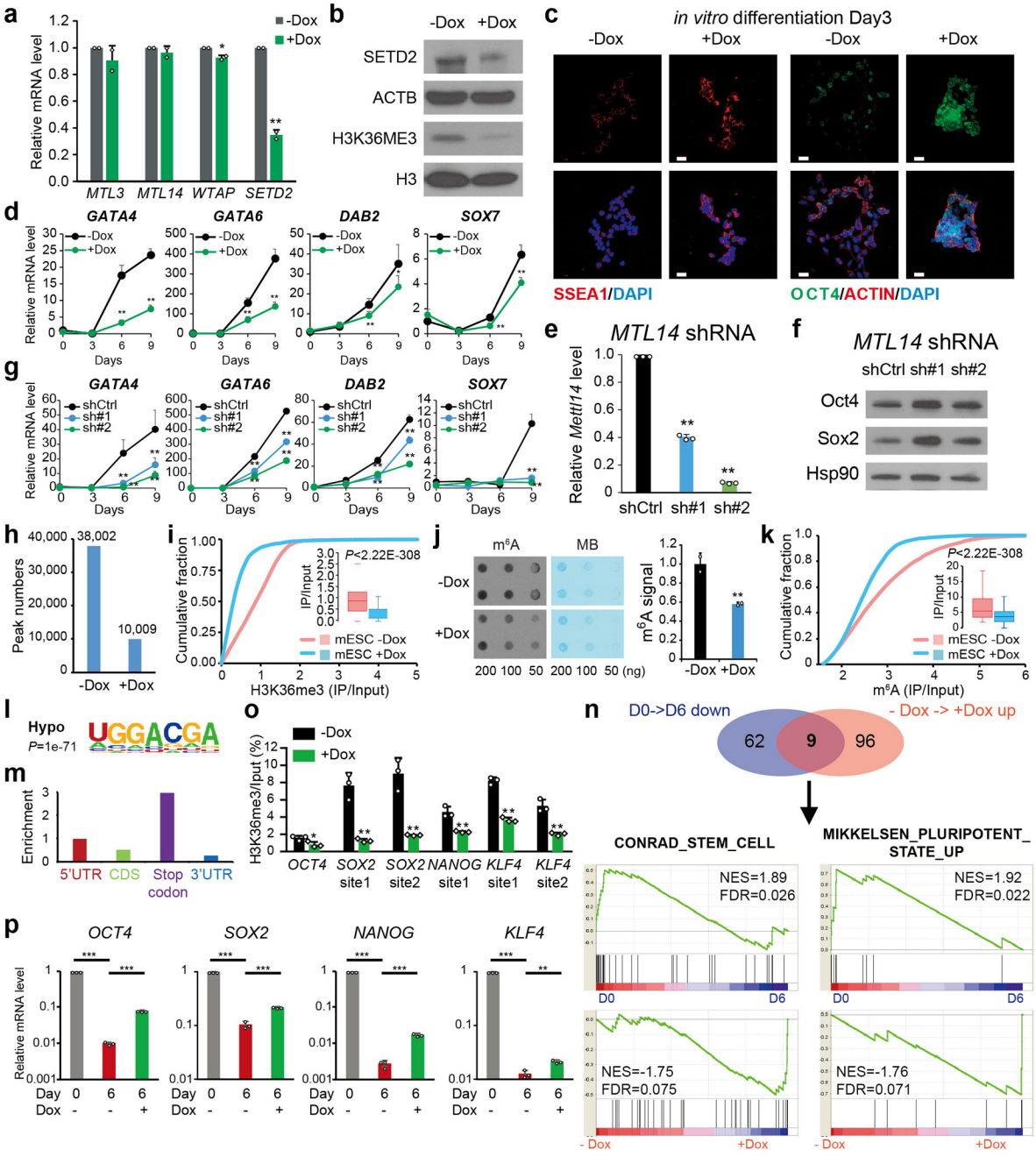

Extended Data Figure 9. Silencing of SETD2 demethylates H3K36me3 and m^{6}A of pluripotency factors and delays the *in vitro* differentiation of mESCs.

(a) qPCR showing remarkable downregulation of SETD2, but not m^{6}A MTC genes, in doxycycline (Dox)-induced Setd2 knockdown mESCs. (b) Western blot showing reduction of Setd2 and decrease of H3K36me3 in doxycycline (Dox)-induced SETD2 knockdown mESCs after 48 hours of Dox treatment. (c) Immunofluorescence showing expression of Stage-specific embryonic antigen-1 (SSEA-1, left) and OCT4 (right) in control (-Dox) and SETD2 knockdown (+Dox) mESCs after 3 days of LIF withdrawal. Scale bar =10 μm. (d) Expression level changes of endoderm differentiation markers during *in vitro* differentiation

of mESCs. (e) Silencing of METTL14 by shRNAs in mESCs as determined by qRT-PCR. (f) Silencing of METTL14 promotes the expression of pluripotency markers in mESCs. HSP90 serves as a loading control. (g) Silencing of METTL14 delayed emerging of endoderm markers in mESCs as determined by qPCR assays. (h) Numbers of H3K36me3 peaks identified in mESCs with or without Dox-induced SETD2 knockdown by ChIP-seq. (i) ChIP-seq revealed global hypomethylation of H3K36me3 in mESCs with doxycyclin treatment as shown by histogram distribution and box plots. For the box plot, top of upper whisker is 95th percentile (shCtrl=2.519, shSETD2=1.081), top of the box is 75th percentile (shCtrl=1.281, shSETD2=0.527), line through the box is median (shCtrl=0.886, shSETD2=0.312), bottom of the box is 25th percentile (shCtrl=0.454, shSETD2=0.155), and bottom of the lower whisker is 5th percentile (shCtrl=0.000, shSETD2=0.000). *P* value was calculated using two-sided Wilcoxon and Mann-Whitney test. (j) Dot blot (left) and quantification (right, values are mean±SD) revealed reduction of cellular m^{6}A in mESCs by doxycycline-induced knockdown of Setd2. (k) m^{6}A-seq revealed global hypomethylation of m^{6}A in mESCs with doxycyclin treatment as shown by histogram distribution and box plots. For the box plot, top of upper whisker is 95th percentile (shCtrl=18.500, shSETD2=10.200), top of the box is 75th percentile (shCtrl=9.530, shSETD2=5.360), line through the box is median (shCtrl=5.480, shSETD2=3.700), bottom of the box is 25th percentile (shCtrl=3.530, shSETD2=2.110), and bottom of the lower whisker is 5th percentile (shCtrl=2.000, shSETD2=0.000). *P* value was calculated using two-sided Wilcoxon and Mann-Whitney test. (l) HOMER motif analysis revealed conserved motifs enriched in hypomethylated peaks. *P* value was calculated by HOMER algorithm. (m) The enrichment of hypomethylated m^{6}A peak distribution. The enrichment fold was determined by the proportion of m^{6}A peaks normalized by the length of the region. (n) Gene set enrichment analysis (GSEA)[58] of downregulated genes upon differentiation (D0 -> D6 down) and upregulated genes upon SETD2 silencing (-Dox -> +Dox up). (o) Determination of H3K36me3 abundance in pluripotency factors by ChIP-qPCR. (p) mRNA levels of pluripotency factors in mESCs as examined by qPCR. Values are mean±SD of two independent experiment in a, or three independent experiments in d, e, g, j, o and p; two-tailed student's t-test; *, P<0.05; **, P<0.01; ***, P<0.001. Images in b, f and j were representative of three independent experiments. Source data of a, d, e, g, j, o and p are in Supplementary Table 4.

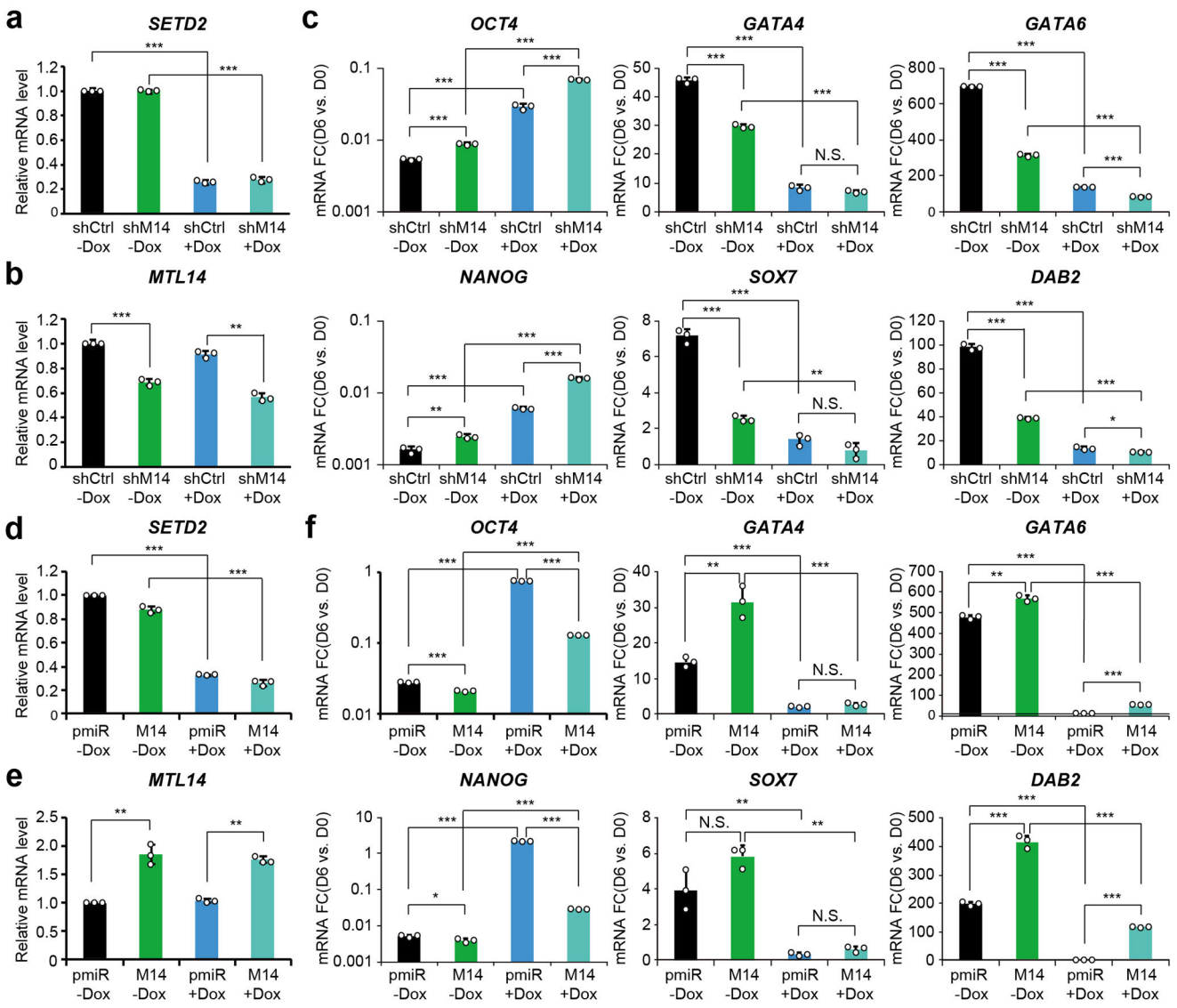

Extended Data Figure 10. Impact of SETD2 and METTL14 in mESCs differentiation.

(a and b) qPCR detecting the expression of *SETD2* (a) and *METTL14* (b) in mESCs. (c) The fold changes (D6 vs. D0) of gene expression of pluripotency factors and differentiation markers during *in vitro* differentiation of mESC with SETD2 and/or METTL14 knockdown. (d and e) qPCR detecting the expression of *SETD2* (d) and *METTL14* (e) showed the knockdown of SETD2 and overexpression of METTL14 in mESCs. (f) The fold changes (D6 vs. D0) of gene expression of pluripotency factors and differentiation markers during *in vitro* differentiation of mESC with SETD2 knockdown and/or METTL14 overexpression. Values are mean±SD of three independent experiments in a, b, c, d, e and f; two-tailed student's t-test; *, $P<0.05$; **, $P<0.01$; ***, $P<0.001$; N.S., non-significant. Source data of a, b, c, d, e, and f are in Supplementary Table 4.

Supplementary Material

Refer to Web version on PubMed Central for supplementary material.

Acknowledgements:

This work was supported in part by the National Institutes of Health (NIH) Grants R01 CA214965 (J.C.), R01 CA211614 (J.C.), R01 CA178454 (J.C.), R01 CA182528 (J.C.), RM1 HG008935 (C.H.), R21 CA187276 (G.H.), R01 CA163493 (J.G.), R35CA197628 (M.M.), U10CA180827 (M.M.), R01CA137060 (M.M.), R01CA157644 (M.M.), R01CA172558 (M.M.) and R01CA213138 (M.M.), and grants 2017YFA0504400 (J.Y.), 91440110 (J.Y.) and 31671349 (L.Q.) from National Nature Science Foundation of China, and Cancer Center Support Grant (P30CA33572) from City of Hope National Medical Center. J.C. is a Leukemia & Lymphoma Society (LLS) Scholar. C.H. is an investigator of the Howard Hughes Medical Institute (HHMI). M.M. is a Howard Hughes Medical Institute (HHMI) Faculty Scholar. B.S.Z. is an HHMI International Student Research Fellow. F.A. was supported by a Deutsche Forschungsgemeinschaft (DFG) fellowship (AU 525/1–1).

References:

1. Egger G, Liang G, Aparicio A & Jones PA Epigenetics in human disease and prospects for epigenetic therapy. Nature 429, 457–463 (2004) [PubMed: 15164071]
2. Wang X et al. N6-methyladenosine-dependent regulation of messenger RNA stability. Nature 505, 117–120 (2014) [PubMed: 24284625]
3. Wang X et al. N(6)-methyladenosine Modulates Messenger RNA Translation Efficiency. Cell 161, 1388–1399 (2015) [PubMed: 26046440]
4. Huang H et al. Recognition of RNA N(6)-methyladenosine by IGF2BP proteins enhances mRNA stability and translation. Nat Cell Biol 20, 285–295 (2018) [PubMed: 29476152]
5. Batista PJ et al. m(6)A RNA modification controls cell fate transition in mammalian embryonic stem cells. Cell Stem Cell 15, 707–719 (2014) [PubMed: 25456834]
6. Wang Y et al. N6-methyladenosine modification destabilizes developmental regulators in embryonic stem cells. Nat Cell Biol 16, 191–198 (2014) [PubMed: 24394384]
7. Geula S et al. m6A mRNA methylation facilitates resolution of naive pluripotency toward differentiation. Science 347, 1002–1006 (2015) [PubMed: 25569111]
8. Xiang Y et al. RNA m(6)A methylation regulates the ultraviolet-induced DNA damage response. Nature 543, 573–576 (2017) [PubMed: 28297716]
9. Li Z et al. FTO Plays an Oncogenic Role in Acute Myeloid Leukemia as a N(6)-Methyladenosine RNA Demethylase. Cancer Cell 31, 127–141 (2017) [PubMed: 28017614]
10. Weng H et al. METTL14 Inhibits Hematopoietic Stem/Progenitor Differentiation and Promotes Leukemogenesis via mRNA m(6)A Modification. Cell stem cell 22, 191–205 e199 (2018) [PubMed: 29290617]
11. Su R et al. R-2HG Exhibits Anti-tumor Activity by Targeting FTO/m(6)A/MYC/CEBPA Signaling. Cell 172, 90–105 e123 (2018) [PubMed: 29249359]
12. Deng X, Su R, Feng X, Wei M & Chen J Role of N6-methyladenosine modification in cancer. Curr Opin Genet Dev 48, 1–7 (2017) [PubMed: 29040886]
13. Meyer KD et al. Comprehensive analysis of mRNA methylation reveals enrichment in 3' UTRs and near stop codons. Cell 149, 1635–1646 (2012) [PubMed: 22608085]
14. Dominissini D et al. Topology of the human and mouse m6A RNA methylomes revealed by m6A-seq. Nature 485, 201–206 (2012) [PubMed: 22575960]
15. Linder B et al. Single-nucleotide-resolution mapping of m6A and m6Am throughout the transcriptome. Nat Methods 12, 767–772 (2015) [PubMed: 26121403]
16. Liu J et al. A METTL3-METTL14 complex mediates mammalian nuclear RNA N6-adenosine methylation. Nat Chem Biol 10, 93–95 (2014) [PubMed: 24316715]
17. Barski A et al. High-resolution profiling of histone methylations in the human genome. Cell 129, 823–837 (2007) [PubMed: 17512414]

18. Pokholok DK et al. Genome-wide map of nucleosome acetylation and methylation in yeast. Cell 122, 517–527 (2005) [PubMed: 16122420]
19. Sun XJ et al. Identification and characterization of a novel human histone H3 lysine 36-specific methyltransferase. The Journal of biological chemistry 280, 35261–35271 (2005) [PubMed: 16118227]
20. Whetstine JR et al. Reversal of histone lysine trimethylation by the JMJD2 family of histone demethylases. Cell 125, 467–481 (2006) [PubMed: 16603238]
21. Carrozza MJ et al. Histone H3 methylation by Set2 directs deacetylation of coding regions by Rpd3S to suppress spurious intragenic transcription. Cell 123, 581–592 (2005) [PubMed: 16286007]
22. Joshi AA & Struhl K Eaf3 chromodomain interaction with methylated H3-K36 links histone deacetylation to Pol II elongation. Molecular cell 20, 971–978 (2005) [PubMed: 16364921]
23. Luco RF et al. Regulation of alternative splicing by histone modifications. Science 327, 996–1000 (2010) [PubMed: 20133523]
24. Dominguez AA, Lim WA & Qi LS Beyond editing: repurposing CRISPR-Cas9 for precision genome regulation and interrogation. Nature reviews. Molecular cell biology 17, 5–15 (2016) [PubMed: 26670017]
25. Kizer KO et al. A novel domain in Set2 mediates RNA polymerase II interaction and couples histone H3 K36 methylation with transcript elongation. Mol Cell Biol 25, 3305–3316 (2005) [PubMed: 15798214]
26. Olmos Y, Hodgson L, Mantell J, Verkade P & Carlton JG ESCRT-III controls nuclear envelope reformation. Nature 522, 236–239 (2015) [PubMed: 26040713]
27. Wienken CJ, Baaske P, Rothbauer U, Braun D & Duhr S Protein-binding assays in biological liquids using microscale thermophoresis. Nature communications 1, 100 (2010)
28. Hacker KE et al. Structure/Function Analysis of Recurrent Mutations in SETD2 Protein Reveals a Critical and Conserved Role for a SET Domain Residue in Maintaining Protein Stability and Histone H3 Lys-36 Trimethylation. The Journal of biological chemistry 291, 21283–21295 (2016) [PubMed: 27528607]

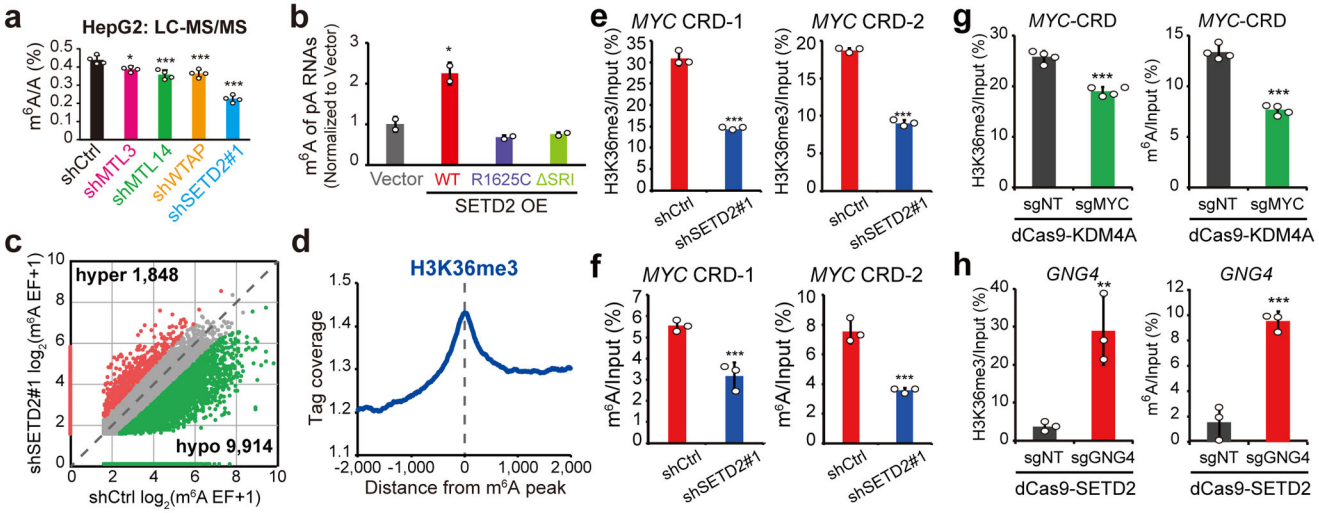

Figure 1. H3K36me3 histone modification affects *de novo* m^{6}A RNA methylation.

(a) LC-MS/MS quantification of m^{6}A abundance in poly(A) RNA from HepG2 cells with knockdown of SETD2 (shSETD2#1) or individual m^{6}A MTC genes. Values are mean±SD of two independent experiments. (b) m^{6}A level of ploy(A) RNA from A498 cells with ectopic expression of wild type (WT) or mutated (R1625C and ΔSRI) SETD2 or empty pEGFP vector. The m^{6}A abundance was determined by dot blot and quantified (values are mean±SD). Note that R1625C-SETD2 is catalytically inactive[28], whereas truncation of the small three-helix domain (ΔSRI-SETD2) impairs the direct binding between SETD2 and Pol II and the co-transcriptional installation of H3K36me3[25]. (c) Scatter plot of m^{6}A peaks in control (shCtrl) and SETD2 knockdown (shSETD2#1) HepG2 cells. The abundance of m^{6}A peaks was calculated as enrichment fold (EF, IP/input) from 3 independent m^{6}A-seq replications. Hypermethylated (hyper) peaks were in red, while hypomethylated (hypo) peaks were in green. (d) Distribution of H3K36me3 relative to the m^{6}A peaks in HepG2 cells. (e and f) H3K36me3 (e) and m^{6}A (f) levels in *MYC* CRD determined by ChIP-qPCR and gene-specific m^{6}A assays in shSETD2#1 and control HepG2 cells. Values are mean±SD of three independent experiments. (g and h) H3K36me3 (left) and m^{6}A (right) level on specific locus were detected in HEK293T cells co-transfected with dCas9-KDM4A (g) or dCas9-SETD2 (h) and specific sgRNAs or non-targeting control (sgNT) as indicated. Values are mean±SD of four independent experiments. Two-tailed student's t-test was used to test difference in a, b, e, f, g and h; *, P<0.05; **, P<0.01; ***, P<0.001. Source data of a, b, e, f, g and h are in Supplementary Table 4.

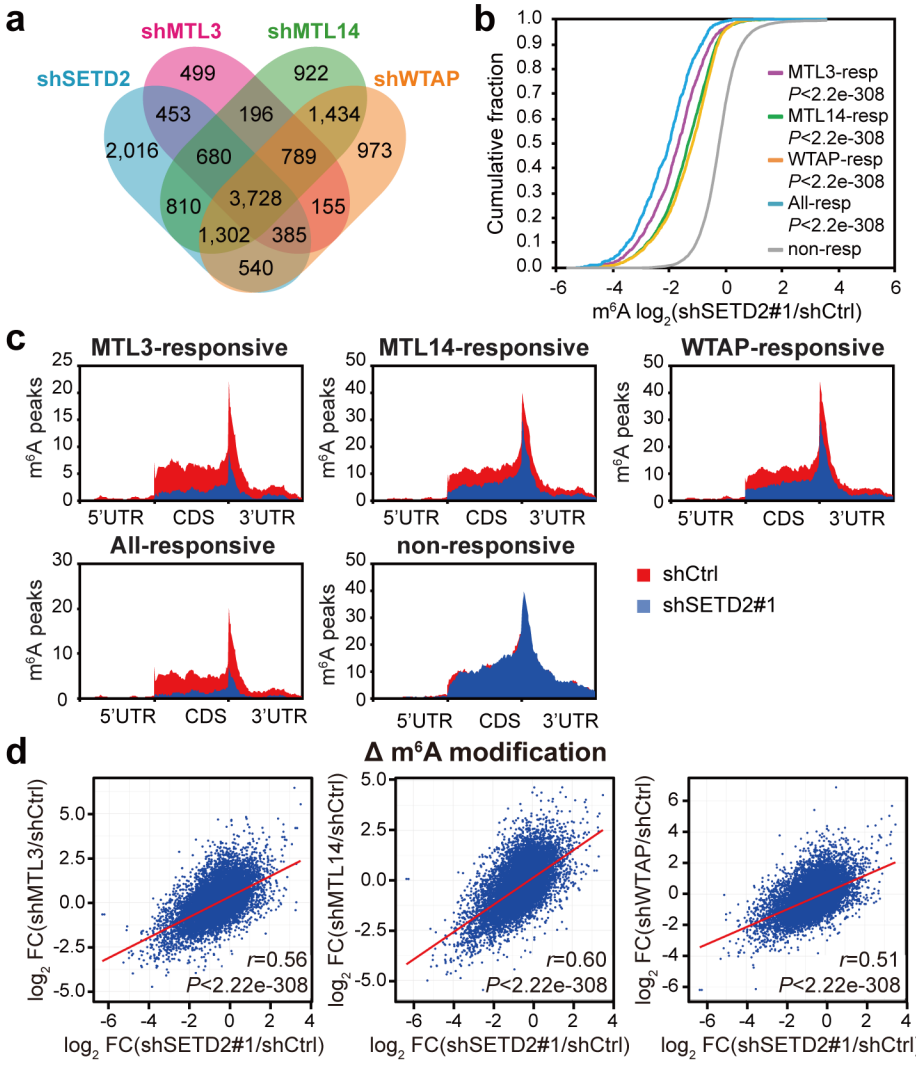

Figure 2. Transcriptome-wide cooperation of H3K36me3 and MTC in m^{6}A regulation

(a) Venn diagram of significantly hypomethylated peaks in HepG2 cells upon knockdown of SETD2 (shSETD2#1) or individual m^{6}A MTC genes. (b) Cumulative curves showing m^{6}A demethylation in m^{6}A MTC gene-responsive peaks upon SETD2 silencing. *P* values were calculated using two-sided Wilcoxon and Mann-Whitney test. (c) Metagene profiles of m^{6}A modifications in MTC gene-responsive peaks and non-responsive peaks. Note that only loci with H3K36me3 modification in the shCtrl cells were included in the analysis. (d) Correlation of fold-change (FC) in m^{6}A abundance between SETD2 knockdown and individual MTC gene knockdown cells. Correlation coefficient (*r*) and *P* values were calculated by Pearson's Correlation analysis.

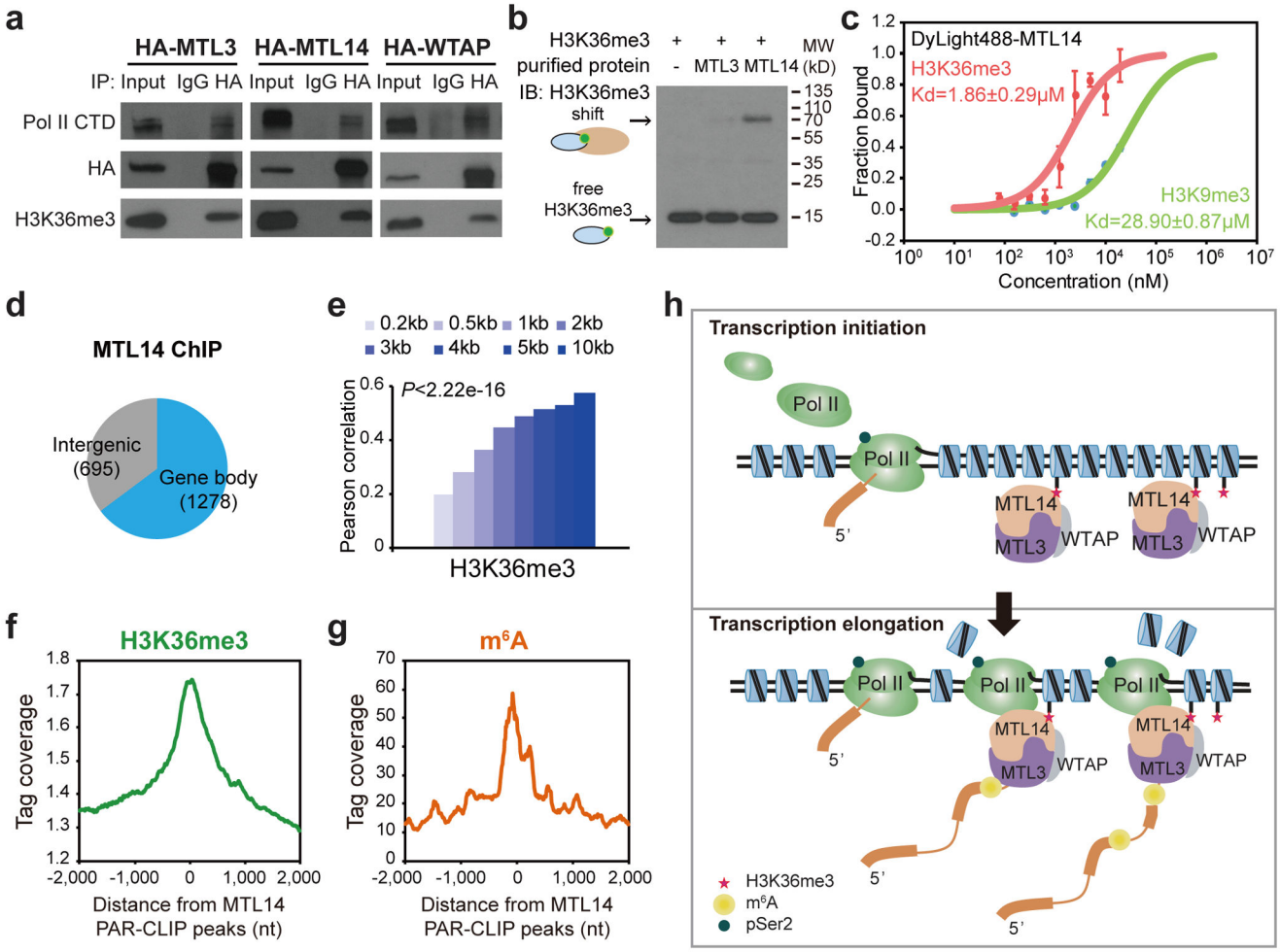

Figure 3. H3K36me3 is recognized by METTL14 and guides m^{6}A modifications co-transcriptionally.

(a) Co-immunoprecipitation and western blot in Hela cells with forced expression of HA-tagged m^{6}A MTC genes. (b) Gel shift of H3K36me3 with recombinant human METTL3 or METTL14 in native SDS-PAGE gel. (c) Binding curves and calculated Kd of DyLight488-METTL14 with full length H3K36me3 or H3K9me3 peptide. Values are mean±SD of three independent experiments for H3K36me3 and two independent experiments for H3K9me3. (d) Distribution of METTL14 binding sites on chromatin identified by ChIP-seq. (e) Pearson correlation coefficients analysis of METTL14 ChIP-seq signals with genomic H3K36me3 features in non-overlapping, non-repetitive windows of different sizes along the genome. (f and g) Distribution of H3K36me3 (f) or m^{6}A (g) relative to nearest METTL14 RNA binding sites identified by PAR-CLIP-seq. (h) Proposed model underlying the mechanism of H3K36me3-guided deposition of m^{6}A methylation. Images in a and b were representative of three independent experiments. Source data of c are in Supplementary Table 4.

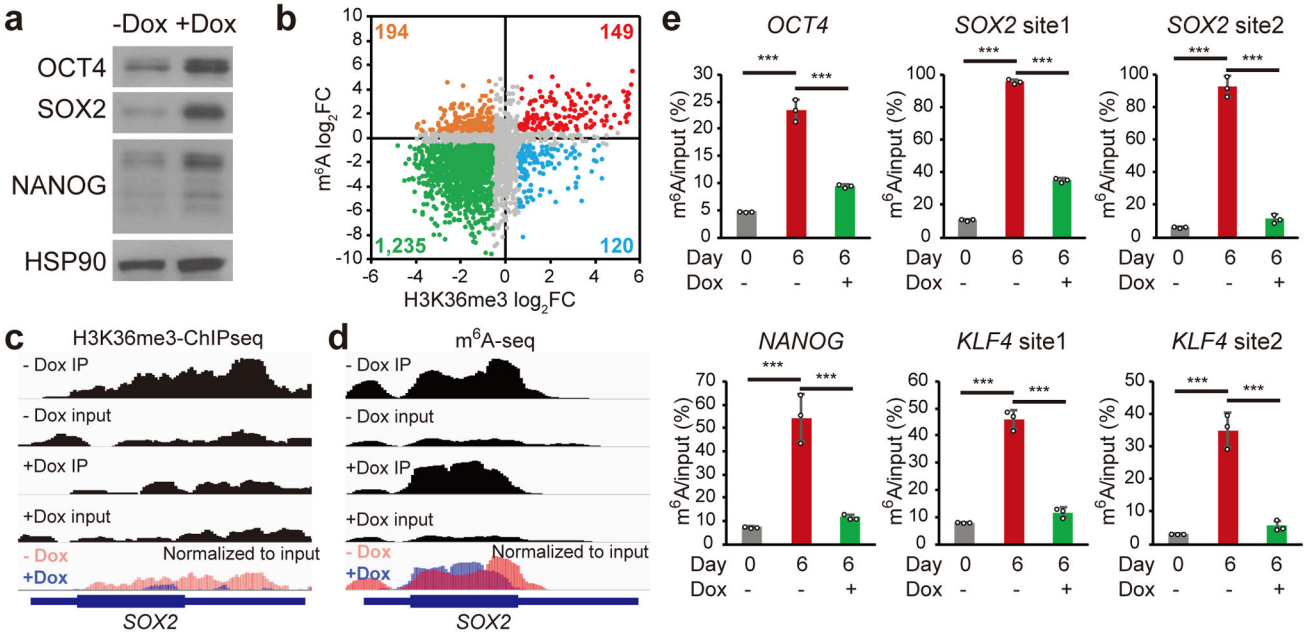

Figure 4. Loss of H3K36me3 reduces m^{6}A in mouse embryonic cells and delays *in vitro* differentiation.

(a) Western blot showing increase of pluripotency factors in mESCs with Dox-induced SETD2 knockdown. (b) Distribution of genes with more than 1.5 fold changes (P<0.05) in both m^{6}A level and H3K36me3 level in SETD2 knockdown mESCs compared to control cells. (c and d) Distribution of H3K36me3 peaks (c) and m^{6}A peaks (d) across *SOX2* mRNA transcript. (e) m^{6}A abundance of individual sites in mRNA transcripts of pluripotency factors during differentiation was determined by m^{6}A-IP and qRT-PCR. Values are mean ±SD of three independent experiments; two-tailed student's t-test; ***, P<0.001. Images were representative of three independent experiments. Source data of e are in Supplementary Table 4.